Sulfonated cryogel scaffolds for focal delivery in *ex-vivo* brain tissue cultures

Dimitri Eigel[1], Romy Schuster[2], Max J. Männel[1], Julian Thiele[1], Martyna J. Panasiuk[3], Laura C. Andreae[3], Carmine Varricchio[4], Andrea Brancale[4], Petra B. Welzel[1], Wieland B. Huttner[2], Carsten Werner[1,5], Ben Newland[1,4]*, Katherine R. Long[2†,3]*

[1] Leibniz-Institut für Polymerforschung Dresden e.V., Hohe Straße 6, D-01069 Dresden, Germany.

[2] Max Planck Institute of Molecular Cell Biology and Genetics, Pfotenhauerstraße 108, D-01307 Dresden, Germany

[3] Centre for Developmental Neurobiology, Institute of Psychiatry, Psychology and Neuroscience, King's College London, London SE1 1UL, United Kingdom; MRC Centre for Neurodevelopmental Disorders, King's College London, London SE1 1UL, United Kingdom. * katie.long@kcl.ac.uk

[4] School of Pharmacy and Pharmaceutical Sciences, Cardiff University, King Edward VII Avenue, Cardiff, CF10 3NB, U.K. * newlandb@cardiff.ac.uk

[5] Technische Universität Dresden, Center for Regenerative Therapies Dresden, Fetscherstr. 105, 01307 Dresden, Germany

[†]Previous address

Keywords: Sulfonated cryogel; biomaterial tool; tissue culture; focal delivery; human brain tissue, mouse brain tissue, neuronal function

Abstract

The human brain has unique features that are difficult to study in animal models, including the mechanisms underlying neurodevelopmental and psychiatric disorders. Despite recent advances in human primary brain tissue culture systems, the use of these models to elucidate cellular disease mechanisms remains limited. A major reason for this is the lack of tools available to precisely manipulate a specific area of the tissue in a reproducible manner. Here we report an easy-to-use tool for site-specific manipulation of human brain tissue in culture. We show that line-shaped cryogel scaffolds synthesized with precise microscale dimensions allow the targeted delivery of a reagent to a specific region of human brain tissue in culture. 3-sulfopropyl acrylate (SPA) was incorporated into the cryogel network to yield a negative surface charge for the reversible binding of molecular cargo. The fluorescent dyes BODIPY and DiI were used as model cargos to show that placement of dye loaded scaffolds onto brain tissue in culture resulted in controlled delivery without a burst release, and labelling of specific regions without tissue damage. We further show that cryogels can deliver tetrodotoxin to tissue, inhibiting neuronal function in a reversible manner. The robust nature and precise dimensions of the cryogel resulted in a user-friendly and reproducible tool to manipulate

primary human tissue cultures. These easy-to-use cryogels offer an innovate approach for more complex manipulations of *ex-vivo* tissue.

1. Introduction

There have been many advances in human cell and tissue culture in the past decade that have allowed great leaps in our understanding of how the human body develops[1–6]. This work has highlighted major differences between humans and animal models, and consequently the necessity of studying human biology in human systems. One area where this is especially true is the development of the human brain that is arguably more complex and far less understood than that of commonly used animal models, such as the mouse[7–9]. Additionally, recent single-cell sequencing work has identified key differences in gene expression and cell composition between primary human brain tissue and 3D human cell culture systems, such as organoids, indicating the need to work with primary tissue where possible[10–14]. However, a major downside of working with human model systems, especially primary tissue, is the comparative lack of tools to pharmacologically or genetically modify the tissue or cells. Specifically, efficient and reproducible targeting of a precise area of primary tissue remains difficult, with options limited to applying a reagent to a tissue area by hand, resulting in a large degree of experimenter-error or uncontrolled spread away from the administration site. This has led to many descriptive studies using human brain tissue, but relatively few exploring the cellular mechanisms underlying the biology observed[7].

To address this issue, new tools need to be developed to allow precise and reproducible manipulation of primary human brain tissue in culture. Biomaterials offer a diverse and easily modifiable technology for the generation of such tools. Whilst hydrogels have been extensively investigated for local drug delivery applications[15–18], cryogels, a subclass of hydrogel, exhibit several favorable properties for use in ex-vivo culture over other their conventional hydrogel counterparts. They are robust with good mechanical stability for ease of handling. Furthermore, they are easily modifiable and can be prepared and stored as a dry material, allowing shape characteristics to be maintained upon de/rehydration.

Cryogels, like hydrogels, are hydrophilic three-dimensional polymeric networks, but are macroporous. These pores are formed because polymerization of the monomers is performed below

the freezing temperature of the solvent (which is commonly water), i.e. in the presence of ice crystals (cryo-polymerization)[19]. Ice crystals act as a porogen, by displacing the liquid monomer phase either before or during polymerization. Large and interconnected pores are generated upon thawing of the solid crystals. The monomer composition and the morphology of the frozen solvent can therefore significantly influence cryogel features such as pore architecture, microstructure, and ultimately the mechanical properties[20,21], allowing easy modification/customization of the material.

Cryogels for applications in tissue engineering and regenerative medicine applications have been synthesized from a wide range of naturally occurring starting materials such as collagen[22–24], agarose[25–27], and heparin[28–30] to name a few. Synthetic poly(ethylene glycol) (PEG) has also been previously used in cryogel design, either in conjunction with the aforementioned materials[29,31–33] or alone[34–36]. PEG offers a relatively inert, charge-neutral, hydrophilic and biocompatible material[24,30], making it a good starting point for our cryogel tool design.

Cryogels can be synthesized to contain cationic (R-NMe_2^+; R_1-NR_3^+), anionic (R-CO_2H; R-SO_3H), or both functionalities (zwitterionics or polyampholytes)[37–39]. Such charged units can be exploited to improve the binding and release of charged guest molecules, such as dyes, drugs, or proteins, via strong electrostatic interactions with the host cryogel. For example, Kudaibergenov et al. created cryogels consisting of the positively charged monomer 2-dimethylaminoethyl methacrylate and the negatively charged monomer methacrylic acid, which allowed the binding and controlled release of molecules such as methylene blue, methyl orange, sodium dodecylbenzene sulfonate, and lysozyme[40]. Additionally, Park et al. demonstrated the use of superporous hydrogels in various potential drug delivery systems[41]. These were modified with anionic functionalities like 2-acrylamido-2-methyl-1-propanesulfonic acid or 3-sulfopropyl acrylate (SPA) for electrostatic host-guest interactions[41,42].

In short, the tunability in cryogel design means that parameters such as surface charge, surface area to volume ratio, and the elastic sponge-like mechanical properties can all be adjusted to suit the intended application. These cryogel features make them an attractive platform technology from which to design highly versatile tools for use in cell and tissue culture applications. Here, we have taken advantage of these characteristics to develop a novel cryogel tool to enable precise and reproducible application of fluorescent dyes to human fetal brain explant and slice cultures. In

addition, we have also demonstrated the applicability of these cryogels for reversible drug delivery to *ex vivo* acute mouse brain slices. We used state-of-the-art soft lithography and a template-assisted synthesis to create microscale cryogels with highly defined dimensions. The incorporation of negatively charged functional groups allowed electrostatic binding and controlled release of molecules with positively charged regions such as BODIPY and DiI dyes. Finally, we have shown that these cryogels can be used to focally label cells within a defined region of the tissue. In the future, these tools will enable the visualization and tracking of individual cells and can be further developed to focally apply pharmacological or genetically modifying substrates to defined regions of the tissue slice.

2. Materials and Methods

2.1. Materials

All chemicals and consumables used for these studies are shown in Table 1 and were used as received unless otherwise stated. Human fetal brain tissue culture media was used in the following composition: 84 ml of neurobasal medium supplemented with 10 ml rat serum (for mouse and ferret cultures) or 10 mL of KOSR (for human cultures), 1 mL glutamine (2 mM), 1 mL Penicillin-Streptomycin (100x), 1 mL N-2 supplement (100x), 2 mL B-27 supplement (50x) and 1 mL of 1 M HEPES-NaOH, pH 7.2, to yield a final volume of 100 mL.

Table 1 – A list of the reagents used with respective suppliers.

Product	**Catalog number**	**Company**
Poly(ethylene glycol) diacrylate (PEGDA, M_n = 700 g/mol)	455008	Sigma Aldrich
3-sulfopropyl acrylate potassium salt (SPA)	251631	Sigma Aldrich
2-hydroxy-2-methylpropiophenone (HMPP)	405655	Sigma Aldrich
Phosphate-buffered saline (PBS)	D8537	Sigma Aldrich
Dimethyl sulfoxide (DMSO)	276855	Sigma Aldrich
Absolute ethanol (EtOH)	1070172511	Sigma Aldrich
Corning Costar TC-treated multiple size 6 well plates	CLS3506	Sigma Aldrich
Dulbecco's Modified Eagle Medium: Nutrient Mixture F-12 (DMEM/F-12)	D8437	Sigma Aldrich
1,1′-dioctadecyl-3,3,3′,3′-tetramethylindocarbocyanine perchlorate (DiI)	468495	Sigma Aldrich
8-chloromethyl-4,4-difluoro-1,3,5,7-tetramethyl-4-bora-3a,4a-diaza-s-indacene (CellTracker™ Green BODIPY®)	C2102	Invitrogen™
Poly(dimethylsiloxane) (PDMS) silicone elastomer kit	184 Silicone	SYLGARD™

ATTO 647-labeled maleimide	AD 647-41	ATTO-TEC
Hydrophilic PTFE cell culture inserts	PICM03050	Merck Millipore
Photopolymer (resin) R11	R11	EnvisionTEC
Neurobasal medium	21103049	Gibco™
KnockOut™ Serum Replacement (KOSR)	10828028	Gibco™
N-2 Supplement (100X)	17502048	Gibco™
B-27™ Supplement (50X), serum free	17504044	Gibco™
HEPES-NaOH (1 M, pH 7.2)	9105.3	CARL ROTH®
Penicillin-Streptomycin-Glutamine (Pen-Strep) (100X)	10378016	Gibco™
Tetrodotoxin citrate	1069	Tocris
Cremophor EL	238470	Sigma
Oregon Green™ 488 BAPTA-1, AM	O6807	ThermoFisher
Pluronic-F127 solution	P6867	ThermoFisher

2.2. 3D printing of the line-shaped master structures

Micro-stereolithography (µSL) was used to fabricate the master structures with line-shaped protrusions. Digital files were designed with Autodesk Inventor Professional 2020 (Autodesk Inc., San Rafael, United States) and the computer-aided design (CAD) file was converted into a standard tessellation language (STL) file. A Perfactory P4 Mini (EnvisionTEC GmbH, Gladbeck, Germany) was used as the 3D-printer. The .stl file was loaded into the printer's software and supporting structures were generated within the software to ensure sufficient adhesion of the printed part to the building platform. The volume of a typical design was around 1 mL. We designed masters with a total size of 10 mm x 21 mm x 5 mm in width, length, and height respectively. Rising from the surface of the masters, we implemented line-shaped protrusions with a fixed length of 10 mm and various cross-section dimensions (width x height) of 150 x 160 µm, 250 x 300 µm, and 450 x 260 µm. These were 3D-printed with a layer thickness of 50 µm within 1 hour using a red-transparent photopolymer formulation R11 (EnvisionTEC, Gladbeck, Germany) as the resin. After the printing process, the uncured resin was removed by washing the 3D-printed masters with isopropyl alcohol (IPA) for 3 minutes in an ultrasonic bath. The masters were then dried at 60 °C for 30 minutes. Finally, the supporting structure was removed, and the master was post-cured using an Otoflash G171 chamber (NK-Optik GmbH, Baierbrunn, Germany).

2.3 Fabrication of line-shaped structured PDMS template

The PDMS templates featuring line-shaped cavities of 10 mm in length, and 150 µm, 250 µm or 450 µm in width and 160 µm, 300 µm or 260 µm in depth, respectively, were created as an inverse

of the 3D printed line-shaped protrusions of the master structures. Therefore, the master structures were covered with the PDMS pre-polymer mixture (PDMS elastomer to crosslinker (4:1)), which was cured at 37 °C for 20 hours. Afterward, the PDMS structure was gently peeled off the master and treated for 10 minutes in the plasma cleaner (Expanded Plasma cleaner, PDC-002 (230 V), Harrick Plasma Inc., Ithaca, NY, USA) to temporarily introduce hydroxide groups at the surface. This hydrophilization made it suitable for aqueous pre-polymer solutions to fill in the line-shaped cavities.

2.4. 3D master and PDMS template characterization by multi-pinhole confocal microscopy

The dimensions and the topography of the 3D printed master structures and the empty and cryogel filled PDMS templates were analyzed via multi-pinhole confocal microscopy utilizing a µsurf explorer (NanoFocus AG, Germany) equipped with a 10x and 20x objective (Olympus, Germany). 3D height maps were generated, and profile sections were recorded using µSoft analysis software (NanoFocus AG).

2.5. Synthesis of line-shaped PEGDA-co-SPA cryogels

The line-shaped PEGDA-co-SPA cryogels were synthesized in PDMS templates via cryopolymerization. An aqueous precursor solution containing PEGDA and SPA monomer at 100 mg/mL (molar ratio 1:1) and 1 mg/mL HMPP as a photoinitiator was freshly prepared prior to use. 4.8 µL, 12.0 µL or 15.2 µL in a total of this solution were added to the respective PDMS template with channel widths of either 150 µm, 250 µm or 450 µm, corresponding to 0.24 µL, 0.75 µL or 1.17 µL per channel, respectively. The filled templates were then placed in a freezer for 30 minutes at a processing temperature of -20°C. Then, each template was exposed to UV light (8 W UV hand lamp, wavelength 254 nm, Benda, Wiesloch, Germany) for 3 minutes whilst still at -20°C. Afterwards, the resulting line-shaped PEGDA-co-SPA cryogels were left to dry for 1 hour in a vacuum oven within the template. Finally, they were removed from their template using forceps and washed two times with absolute ethanol and two times with Milli-Q water to remove unbound monomers and photoinitiator. To analyze the effect of SPA content on loading/release properties, cryogels were produced that contained different amounts of SPA according the PEGDA/SPA molar ratios 50:50 (as above), 75:25 and 95:5. Cryogels consisting of PEGDA alone were produced in the same manner as above, but without the SPA monomer (PEGDA/SPA molar ratio 100:0). The

concentration of the monomer precursor solutions was kept at 10 mg/mL and all other parameters remained the same as above.

2.6. Synthesis of PEGDA-co-SPA control hydrogels

An attempt to make line shaped conventional hydrogels from PEGDA-co-SPA was carried out using the parameters described above, but without cryopolymerization. The precursor solution was crosslinked within the template without a prior freezing step.

2.7. Characterization of the mechanical properties of PEGDA-co-SPA cryogels in comparison to conventional hydrogels.

Uniaxial compression tests were performed on 9 mm diameter and 3 mm height PBS swollen PEGDA-co-SPA cryogels and conventional hydrogels of the same size and chemical composition, at room temperature under atmospheric conditions by using an ARES G2 Rheometer (TA Instruments, New Castle, DE, U.S.A.). Samples were compressed between two parallel plates (stainless steel, diameter 8 mm) with a constant linear compression rate of 1 mm/min. The compressive modulus (*E*) of the cryogels was calculated via equation (1) using the uniaxial stress ($\Delta\sigma$) and strain ($\Delta\varepsilon$) parameters from the linear region of the compression curves at low strain regions (0–10%) that were obtained through five independently performed experiments.

$$E = \frac{\Delta\sigma}{\Delta\varepsilon} \tag{1}$$

2.6. Cryogel characterization by Raman spectroscopy and Fourier-transform infrared spectroscopy (FTIR)

The Raman spectra of the line-shaped PEGDA-co-SPA cryogels were recorded and baseline corrected with the Raman Imaging System alpha300R (WITEC, Ulm, Germany) in the 600–1900 cm^{-1} frequency range (excitation wavelength: 785 nm, laser power: 130 mW, objective: 20x (Zeiss), integration time: 0.5 s, accumulation per spectrum: 200). The spectra of the PEGDA monomer, the SPA monomer, and the precursor solution, which contained the monomer and photoinitiator, were used as references.

Infrared spectra of the line-shaped PEGDA-co-SPA cryogel networks were baseline corrected (elastic band method) using a FTIR microscope Hyperion 2000 coupled with a Bruker Vertex 70v (Billerica, USA) and equipped with a single reflection diamond attenuated total reflectance probe

(ATR, Ge-crystal) system from SPECAC (Orpington, U.K.) in the 600–4000 cm^{-1} frequency range (MCT-detector, resolution = 4 cm^{-1}, 100 scans per measurement).

2.7. Scanning electron microscopy (SEM) analysis of the cryogels

Surface and pore morphological features of the line-shaped PEGDA-co-SPA cryogels were visualized using a XL30 ESEM-FEG microscope (Philips, Netherlands) in high vacuum mode with an accelerating voltage of 5 kV. Samples were fixed to aluminum stubs with double-sided adhesive carbon conductive tape and subsequently sputter-coated with gold using a SCD 050 sputter coater (BAL-TEC, Germany) for 60 s at 40 mA.

2.8. Confocal laser scanning fluorescence microscopy (CLSM) analysis of the cryogels

CLSM was used to visualize and measure the pore size of the line-shaped PEGDA-co-SPA cryogels in the hydrated state in phosphate-buffered saline (PBS). To visualize the pores, the cryogels were labeled by adding 0.1 mg/mL of ATTO 647-labeled maleimide to the precursor solution, followed by a subsequent photochemical crosslinking as described above. CLSM was performed with a Dragonfly (Andor Technology, U.K.) mounted on a Nikon Ti-E inverted microscope with a 637 nm laser and diode. Images were taken with either a 10x magnification objective (CFI Plan Apo Lambda, Nikon) or a 20x magnification objective (CFI Plan Apo Lambda, Nikon). For quantitative pore size analysis, 10 z-stacks (70 µm depth, 2 µm step size) were taken per cryogel width type, measuring a total of 400 pores for each cryogel type in both x- and y-directions using ImageJ software (NIH). For qualitative images, 80 µm and 100 µm z-stacks with a step size of 1 µm were acquired.

To visualize the loading and distribution of BODIPY or DiI dyes, the cryogels were incubated in either 0.5 mM BODIPY or 2 mM DiI (prepared in PBS containing 10% DMSO) for 5 min at 37°C. Subsequently, the BODIPY or DiI soaked cryogels were carefully blotted with a lint-free tissue to remove the excess and thus unbound dye. Microscopy analysis was carried out using the 488 nm, 561 nm, and 637 nm laser diodes and images were taken with either a 10x magnification objective (CFI Plan Apo Lambda, Nikon) or a 20x magnification objective (CFI Plan Apo Lambda, Nikon). The images were recorded as 100 µm z-stacks with a step size of 1 µm.

2.9. Swelling measurements

Swelling studies were carried out in PBS (pH 7.4) at 37 °C. Before swelling, the dry cryogels were scanned with the fluorescent image analyzer FLA-5000 (Fujifilm, Japan) and the average widths were measured for every line-shaped cryogel by a three-point determination method using the Multi Gauge analysis software (Fujifilm, Japan). Afterwards, the line-shaped cryogels were immersed in 2 mL of PBS for 24 h at 37 °C until the equilibrium was reached. The final width of the swollen line-shaped cryogels was measured immediately after the removal of excess PBS from the cryogel surface. At least six independent experiments were carried out (n = 6). The volume swelling degree Q_w for the cryogels was obtained from the width of the swollen *w* and the dry cryogel d_0 via Eq. (1) The changes in lengths of the dry cryogels in comparison to the swollen cryogels were also determined by light microscopy.

$$Q_v = \left(\frac{w}{w_0}\right)^3$$

2.10. Dye loading and release analysis

Cryogels (n=4 for each width type) were incubated in 100 µL of BODIPY or DiI solution (0.5 mM and 2 mM respectively in PBS with 10% DMSO, termed the loading stock solution), for 5 minutes at 37°C. BODIPY or DiI soaked cryogels were then carefully blotted with a lint-free tissue to remove the excess dye and immediately placed individually on 30 mm diameter PTFE cell culture inserts (0.4 µm pore size) in six-well plates containing 1 mL of fresh DMEM/F-12 cell culture medium per well. This set-up was used to mimic the application of the line-shaped cryogels to cultured neocortical brain tissue. The amount of loaded BODIPY and DiI was determined by two methods: i) measuring the reduction in volume of the 100 µL loading solution (induced by swelling of the cryogel network and filling of the pores), and ii) measuring the reduction in fluorescence intensity/concentration (described below) of the loading solution (caused by electrostatic loading of the cargo to the cryogel hence depleting the dye in solution).

To measure how much BODIPY or DiI was released from the cryogel to the medium below the insert (incubated at 37 °C), 200 µL of the undernatant was removed (stored at -20 °C) and replaced with fresh cell medium at various time points. For both loading and release experiments, the concentration of the dyes in the loading solution/release medium was determined fluorometrically using a microplate reader Spark® (Tecan Trading AG, Switzerland, BODIPY excitation wavelength λ_{exc} = 522 nm and emission wavelength λ_{em} = 567 nm, DiI excitation wavelength λ_{exc} = 535 nm and emission wavelength λ_{em} = 580 nm) in comparison to a standard curve. The amount

of BODIPY and DiI removed at each time point was factored into the calculation of the total BODIPY and DiI release.

The analysis of cryogels with varying SPA contents was carried out as above but with line-shaped PEGDA-co-SPA cryogels with SPA contents of 0%, 5%, 25% and 50% (n = 3 for each SPA content type with a width of 450 µm).

2.11. Tetrodotoxin (TTX) loading and release analysis from line-shaped PEGDA-co-SPA and PEGDA cryogels

Line-shaped PEGDA-co-SPA cryogels or PEGDA cryogels (n = 3 for each SPA content type with widths of 250 µm or 450 µm) were incubated in 100 µL of TTX (1 mM, dissolved in Milli-Q water, termed the loading solution), for 5 minutes at 37°C. TTX soaked cryogels were then carefully blotted with a lint-free tissue to remove the excess toxin and immediately placed individually on 30 mm diameter PTFE cell culture inserts (0.4 µm pore size) in six-well plates that contained 1 mL of Milli-Q water each. The amount of loaded TTX was determined by measuring the UV absorption intensity of the final loading solution (i.e., determine if electrostatic loading was taking place and thus depletion in concentration) and subtracting this from the initial UV absorption intensity of the TTX loading solution. In order to determine TTX via UV spectroscopy, the TTX loading stock solution was incubated with 2 M NaOH for 45 minutes at 100 °C [43]. In this process, the C_9 base 2-amino-6-hydroxymethyl-8-hydroxyquinazoline formed by alkali hydrolysis is UV active[43,44]. After cooling the loading stock solution to room temperature, the C_9 base can be detected as a shoulder via UV spectroscopy around 276 nm[44]. In order to detect how much TTX was released from the cryogels to the Milli-Q water below the insert (incubated at 37 °C), 200 µL of the undernatant was removed and replaced with fresh Milli-Q water at time points of 10, 20, 30 minutes, followed by 1-24 hours. The collected volumes were stored at -20 °C until analyzed by UV spectroscopy using a microplate reader Spark® (Tecan Trading AG, Switzerland, TTX absorption wavelength $\lambda_{abs.}$ = 271 nm) in comparison to a standard curve. The amount of TTX removed at each time point was considered in the calculation of total TTX release.

2.12. In silico analysis of dye interaction with PEGDA-co-SPA or PEGDA

Molecular modelling experiments were performed using an Asus WS X299 PRO Intel® i9-10980XE CPU @ 3.00GHz × 36 running Ubuntu 18.04 (graphic card: GeForce RTX 2080 Ti).

Molecular Operating Environment (MOE, 2019.10, Montreal, QC, Canada) software was used to build the geometry of the PEGDA-co-SPA polymer model to match the molar ratio used for the cryogel synthesis (1:1 M ratio PEGDA: SPA), for a total of 20 PEGDA-SPA repeat unit (20 KDa). The initial polymer network was optimised using molecular dynamic simulations (Desmond package, Maestro v 11.4, Schrödinger LLC, New York, NY, 2017) in order to identify the most stable conformation of the PEGDA-co-SPA model. Molecular dynamics simulations were performed using OPLS3e force-field in the explicit solvent and the TIP3 water model. A cubic water box was used for the solvation of the system, ensuring a buffer distance of approximately 15 Å between each box side and the polymer model. The systems were neutralised, adding 20 sodium counter ions. A 100 ns molecular dynamic simulation was performed, with a constant temperature (300 K) and pressure (1 atm). All other parameters were set using the Desmond default values. Data were collected every 1 ns. The simulation was performed in triplicate, using a random seed as a starting point each time. Hierarchical clustering based on structural root-mean-squared distance (RMSD) was used to group the different polymer conformations and to select a representative structure for subsequent determination of dye interactions with the model PEGDA-co-SPA construct. A separate model was also designed and constructed as above but containing 20 repeat units of PEGDA alone without an SPA moiety.

The interaction of BODIPY or Dil with the polymer models was analysed using the same experimental conditions. A ratio of 0.1 BODIPY or 0.7 DiI molecules were used per PEGDA-SPA repeat unit, to match the experimental studies. The simulations of drug-polymer interactions (dynamic/reversible loading and release) were performed using the Desmond package. The size of the water box was 20 Å between each box side and the polymer-dye complex, using the same settings described above. The initial dye position was randomly assigned close to the polymer surface, and the dye-polymer interactions were determined by evaluating the variation of the total solute energy of the complex (dye molecule + PEGDA-SPA or PEGDA polymer) with regards to the simulation time (500 ns).

2.13. Mouse brain tissue

Mice used were C57BL/6JOlaHsd and CD1 wild-type animals. E0.5 was set at noon of the day on which the vaginal plug was observed. Experiments were performed in the dorsolateral neocortex of embryonic day (E)14.5 embryos and postnatal day (P)5-7 pups. Images were acquired and

analyzed from coronal sections of the frontal and parietal neocortex. All animal procedures were approved by the appropriate ethical committee (German Animal Welfare Legislation and Home Office, UK), performed (for P5-7 experiments) according to the UK Animals (Scientific Procedures) Act 1986 under personal and project licences held by the authors and met the guidelines of the local and European regulations and the standards for Use of Laboratory Animals.

2.13.1 E14.5 embryonic mouse brain tissue

E14.5 embryonic mouse brains were dissected in PBS and meninges were removed. Cryogels were loaded with CellTracker™ Green BODIPY™ Dye, which was used at 0.5 mM, then placed onto the cortical surface and left for 10-20 minutes. Brains were then fixed for at least 24 hours at 4°C in 4% (wt/vol) paraformaldehyde (PFA) in 120 mM phosphate buffer (pH 7.4).

2.13.2 P5-7 postnatal mouse brain tissue

P5-7 postnatal mouse brains were dissected in ice-cold sucrose artificial cerebrospinal fluid (ACSF), in mM: 240 sucrose, 5 KCl, 1.25 Na_2HPO_4, 26 $NaHCO_3$, 10 glucose, 2 $MgSO_4$, 1 $CaCl_2$. All ACSF solutions were adjusted for a final pH of 7.4 and total osmolarity of 310-320 mosmol l^{-1}. Coronal 300 µm cortical brain slices were obtained using a Leica VT1000 S Vibratome as described in [45]. Slices were then kept in recovery ACSF (125 NaCl, 5 KCl, 1.25 NaH_2PO_4, 26 $NaHCO_3$, 20 glucose, 2 $MgSO_4$, 2 $CaCl_2$) and perfused with carbogen (95% O_2, 5% CO_2) at 24°C for at least 1 hour.

2.13.3 Calcium dye loading and cryogel-TTX application

The calcium dye loading protocol was based on [46]. Slices were placed in 3 mL HEPES ACSF (92 NaCl, 2.5 KCl, 1.25 NaH_2PO_4, 40 $NaHCO_3$, 20 HEPES, 25 glucose, 2 $MgSO_4$, 0.5 $CaCl_2$) and 8 µL of 0.05% Cremophor EL (Sigma) in DMSO at 52°C for 3 minutes. For dye loading, 25 µg Oregon Green 488 BAPTA-1 AM solution (OGB-1, ThermoFisher) was dissolved in 10 µL of dimethyl sulfoxide (DMSO) and added to 10 µL of 2% Pluronic-F127 solution (ThermoFisher) in DMSO. This 20 µL was then pipetted onto the brain slices placed in 5 mL of HEPES ACSF for a final concentration of 2.9 mM OGB-1, 32 µM Pluronic F-127, and 0.004% (v/v) DMSO. The slices were incubated at 40°C for 45 minutes.

As baseline neuronal activity is low in slices due to denervation, we used a modified ACSF (mACSF) containing higher [K+] (69 NaCl, 60 KCl, 1.25 NaH_2PO_4, 26 $NaHCO_3$, 20 glucose, 2 $CaCl_2$). Slices were transferred into mACSF and cryogels loaded with either mACSF (control) or 1 mM tetrodotoxin (TTX), placed onto the brain tissue slice for 2 minutes (using forceps, see Supplemental Video V1) and then removed. Following imaging, slices were then washed in mASCF to remove the TTX for 1 minute before the above steps were repeated in the same area of the brain slice. Images were taken every 20 seconds using a Cairn custom designed dissection microscope.

2.14. Human fetal brain slice culture

Human fetal brain tissue was obtained from the Human Development Biology Resource (HDBR), provided by the Joint MRC/Wellcome Trust (grant # 099175/Z/12/Z) Human Developmental Biology Resource (www.hdbr.org). The HDBR provided fresh tissue from fetuses aged 12-20 post-conception weeks (pcw): 12 pcw, n = 1; 14 pcw, n = 1; 17 pcw, n = 2; 20 pcw, n = 2. Human fetal brain tissue was dissected in PBS and used immediately for culture, cryogel experiments, or fixation. Cryogels were loaded with DiI, which was used at 2 mM, and/or CellTracker™ Green BODIPY™ Dye, which was used at 0.5 mM, then placed onto the tissue. Tissue was cultured as previously described [47]: placed into a rotating flask with 1.5 ml media outlined in 2.1, and incubated at 37°C in the presence of humidified 40% O_2 / 5% CO_2 /55% N_2. All tissue was fixed for at least 24 hours at 4°C in 4% (wt/vol) paraformaldehyde (PFA) in 120 mM phosphate buffer (pH 7.4).

For analysis of tissue damage with SPA and neutral cryogels, 2 mM DiI was pipetted onto human fetal brain tissue and incubated at 37ºC for 30 minutes in the presence of humidified 40% O_2 / 5% CO_2 /55% N_2. The tissue was then thoroughly washed for 10 minutes to remove any remaining DiI on the tissue surface. SPA and neutral cryogels were then loaded with PBS and placed onto the DiI labelled area of the tissue for 2 minutes. The cryogels were then removed from the tissue (using forceps, see Supplemental Video 2) and immediately imaged on a Cairn Custom designed dissection microscope.

For comparison of free-hand application of BODIPY to the cryogels, cryogels were loaded with 2.7 µL of 0.5 mM BODIPY and placed onto the tissue for either 10 or 20 minutes. Images were taken at the time of application, immediately before cryogel removal and after cryogel removal

using a Cairn Custom designed dissection microscope. 2.7 µL of 0.5 mM BODIPY was also pipetted onto the surface of the tissue (i.e., free-hand application without cryogels). Images were taken during the application and after either 10 or 20 minutes. This tissue was then was fixed for at least 24 hours at 4°C in 4% (wt/vol) paraformaldehyde (PFA) in 120 mM phosphate buffer (pH 7.4) and sectioned to analyze the depth of dye penetration.

2.15. Imaging and sectioning of mouse and human tissue

Whole brains and whole mount sections were imaged using a Zeiss Axio Imager.Z1 and ApoTome I or a Cairn Custom designed dissection microscope. Brains were then sucrose-treated (15% and 30% sucrose solution sequentially for each 24 hours) and OCT-embedded and then 20 µm thick sections were cut using a cryostat. These sections were then stained using DAPI (Sigma, 1:1000) and mounted in Mowiol (Merck Biosciences). Sections were then imaged using either a Zeiss LSM 700 or LSM 800 inverted confocal microscope and a Zeiss Plan-Apochromat 20x 0.8 objective. Images shown are maximum intensity projections of 11 optical sections from a 10 µm z-stack.

2.16. Quantification and statistical analysis

All image analyses and quantifications were conducted using Fiji, and all statistical analyses were conducted using GraphPad Prism. Integrated density measurements were conducted using a specified region of interest taken at least three times within the required area and then averaged. All datasets were tested for Gaussian distribution (Kolmogorov-Smirnov test) prior to the selection of the appropriate statistical test. All datasets were analyzed blind. For all graphs, error bars represent either ± standard deviation or standard error of means as stated in the figure legend. Differences between groups were analyzed using a t-test or two-way ANOVA with Bonferroni´s multiple comparison post-hoc test. Data were considered significant if $*P < 0.05$, $**P < 0.01$, $***P < 0.001$ or $****P < 0.0001$.

3. Results

3.1. Synthesis and characterization of line-shaped PEGDA-co-SPA cryogels

Macroporous line-shaped PEGDA-co-SPA cryogel scaffolds were successfully created by a cryogelation process based on a free radical photopolymerization reaction performed at a subzero

processing temperature (-20 °C) within PDMS templates. **Figure 1** and **Figure 2** show schematic representations of the template fabrication process and cryogel synthesis procedure. The characterization of the line-shaped 3D printed masters and the successfully fabricated PDMS templates via confocal multi-pinhole microscopy is provided in supplementary **Figure S1**. The line-shaped PDMS templates were all an inverse of the 3D printed master structure containing line-shaped cavities with widths of 150 µm, 250 µm and 450 µm and a length of 10 mm for each line.

Scanning electron microscopy images (**Figure 2D** and **Figure 3B, C, E, F,** and **3H, I)** show the cryogel morphology in the dry state within the PDMS template, revealing interconnected macropores throughout the cryogel. The resulting dimensions of the three line-shaped cryogel types, dry within the template were 150 x 75 µm (width x height), 250 x 250 µm and 450 x 160 µm as determined by multi-pinhole confocal microscopy profile section analysis (**Figure 3A, D, G**). By using a small amount of ATTO-647 maleimide in the precursor solution to fluorescently label the cryogels, CLSM analysis could be implemented to study the pore structure in the PBS swollen state (application relevant situation). It should be noted that the wavelength of UV light chosen for the photoinitiation (366 nm) did not photo-bleach the far-red (647 nm) ATTO dye selected for the cryogel functionalization. Once the cryogels were placed in PBS, they became swollen to the full depth and also increased in length and width (**Figure 4** and **supplementary Figure S2**). The volume swelling degree of the differently sized cryogels was almost identical since they all consist of the same crosslinked material (PEGDA and SPA) (**supplementary Figure 2A**). In general, all three line-shaped cryogels can also be simply dried and stored under dry state conditions and re-swollen at any time as required.

The mechanical properties of PEGDA-co-SPA cryogels were investigated via uniaxial compression analysis in comparison to conventional hydrogels formed from the same precursor solution but without cryogelation. The hydrogel network ruptured at 40% strain with considerably less stress than the corresponding cryogels could tolerate (**supplementary Figure S3A, B, C**)**.** The cryogels were softer with a lower Young's modulus (8.7 ± 1.6 kPa) than the hydrogel of matching chemical composition (29.5 ± 4.3 kPa) yet would withstand a strain of 80% before failure (**supplementary Figure S3C, D**). This robust nature of the PEGDA-co-SPA cryogels allowed them to be easily removed from the line-shaped cavities in the template, where the corresponding hydrogels were impossible to remove mechanically (**supplementary Figure S4, video V3, V4**).

In agreement with the SEM investigations, the CSLM analysis (**Figure 4**) also verified the macroporous and sponge-like morphological network characteristics in all line-shaped cryogel samples. By varying the template size, the resulting cryogel and its pore size distribution can be accurately controlled as demonstrated in **Figures 3** and **4**. In this respect, the 150 µm width cryogels show the tightest pore size distribution, while the distribution of the 250 µm width cryogels is larger (**Figure 4D**). However, due to comparatively close widths, both cryogels types exhibit similar average pore diameters of 30 µm and 36 µm respectively**.** By comparison, the 450 µm width cryogels show the broadest pore size distribution between 10-100 µm (**Figure 4D**) with an average pore diameter of 67 µm. In summary, confocal multi-pinhole microscopy, SEM, and CLSM studies confirmed that three different line-shaped cryogel sizes could be produced with a macroporous structure and therefore a high surface to volume ratio.

3.2. Chemical characterization of PEGDA-co-SPA cryogels via Raman and FTIR spectroscopy reveals complete crosslinking and the incorporation of negatively charged sulfonate groups

Raman and FTIR spectroscopy analysis of the unlabeled PEGDA-co-SPA line-shaped cryogels were performed as complementary methods in comparison to the pure monomers (**supplementary Figure S5A, B**). These two methods allow the confirmation of a successful crosslinking of PEGDA with SPA in the resulting cryogel scaffolds. The spectral analyzes of Raman and FTIR confirmed complete crosslinking of the polymer network in the cryogel by showing the absence of characteristic vinyl C=C (1636 cm^{-1}, Raman; 1637 cm^{-1}, FTIR) and vinyl CH_2 (1410 cm^{-1}, Raman). Furthermore, the presence and therefore, incorporation of the characteristic sulfonate group ($R\text{-}SO_3^-$) vibrations of SPA (531 cm^{-1}, 1063 cm^{-1} Raman; 1040 cm^{-1}, 1170 cm^{-1} FTIR) were present in the cryogel spectra. This can be observed by a visible shift from 1063 cm^{-1} to 1044 cm^{-1} in the Raman spectrum and a change in intensity at 1040 cm^{-1} and 1170 cm^{-1} in the FTIR spectrum. Additionally, the characteristic C=O vibration of the PEGDA and SPA ester groups (1723, 1719 cm^{-1}, Raman; 1720 cm^{-1}, FTIR) is reduced in intensity and shifted (1732 cm^{-1}, Raman; 1728 cm^{-1}, FTIR) after the cryogelation was performed. These results suggest a complete covalent crosslinking of PEGDA with SPA within the cryogel network, since no free vinyl groups remain in the structure. Also, due to the use and incorporation of the SPA monomer into the cryogel structure, S-O vibrations of the sulfonate group are visible in the cryogel spectra.

3.3. PEGDA-co-SPA based line-shaped cryogels load and release BODIPY and DiI

The commercially available acrylic acid monomer 3-sulfopropyl acrylate (SPA) is a good candidate molecule for incorporating negatively charged moieties into a network structure due to its highly hydrophilic sulfonate functionality. We therefore synthesized macroporous line-shaped PEGDA-co-SPA cryogels to electrostatically bind and release the dyes BODIPY and DiI in a controlled manner. Both these dyes contain positively charged moieties and CSLM showed that they could be loaded to the negatively charged cryogels with an even distribution across the structure (**Figure 5B-D** and **5F-H**). **Figure 5A** and **5E** illustrate the proposed electrostatic attraction between the positively charged nitrogen-containing groups, either within the indocarbocyanine structure of DiI or within the dipyrromethene structure of BODIPY, and the negatively charged sulfonate functionalities of the cryogels. After incubation of the cryogels with the dyes, a significant color change was noted due to the intense red-purple and orange color of DiI and BODIPY respectively (**Figure 6C** and **6F**).

When the line-shaped cryogels were placed into loading solutions, then removed, the volume of the solution was reduced due the cryogel soaking up the solution as it swells. This volume reduction was typically less than 1 µL for 100 µL of loading solution so was not measured experimentally. However, we also observed a significant reduction in the dye concentration in this loading solution after dye loading to the cryogel had taken place (**Figure 6A** and **6D**). This indicates that the dye is drawn out of solution onto the pore walls (struts) of the cryogels through electrostatic attraction. For both dyes, the amount of dye loaded increases with increasing cryogel size (BODIPY amount loaded: 0.99 µg (150 µm width cryogel), 1.91 µg (250 µm width cryogel) and 3.80 µg (450 µm width cryogel); DiI amount loaded: 26.9 µg (150 µm width cryogel), 37.0 µg (250 µm width cryogel) and 55.5 µg (450 µm width cryogel)).

To substantiate the role of SPA in the electrostatic loading of the dye molecules to the cryogels, *in silico* analysis of two molecular models was carried out. One with PEGDA-co-SPA in a 1:1 molar ratio (as used for the experiments) and another just containing PEGDA. By adding the same molar ratio of BODIPY or DiI molecules to the PEGDA-co-SPA unit of the molecular model as was used for the loading and release experiments above, we could observe the total energy of the system. The PEGDA alone model resulted in a total energy of -30.26 KCal/mol (BODIPY) or – 30.87 KCal/mol (DiI). Whilst the addition of SPA to the model (PEGDA-co-SPA) resulted in little

change to the total energy of the system with BODIPY (-31.95 KCal/mol), a large decrease was observed with DiI (-132.43 KCal/mol) indicating strong stabilization through electrostatic interaction. Furthermore, analysis of the interaction between the dye molecules and the molecular model over a period of 500 nanoseconds showed reversible binding of both dye molecules shedding light on the dynamic process of dye loading and subsequent release (**supplementary Figure S6**).

To avoid flooding cultured tissue in later experiments, a slow release of the loaded dye was desirable. A burst release, of large quantities of dye, would ruin precision targeting of specific brain regions. Experimental analysis of the line-shaped PEGDA-co-SPA cryogels showed that only a small amount of the dye was released over the 30-minute analysis period (**Figure 6B** and **6E**)**.** As expected, the amount of dye released tended to be larger from the bigger scaffolds. For instance, the 150 µm width cryogels released 0.72 µg BODIPY and 0.87 µg DiI while in comparison the 450 µm width cryogels released 1.22 µg of BODIPY and 1.08 µg of DiI. The percentage of loaded dye released depends on the strength of the electrostatic host-guest interaction, with a greater percentage of loaded BODIPY being released than DiI (**supplementary Figure S7A, B**). The presence of both negative and positive regions within BODIPY would explain the reduced electrostatic interaction in the *in silico* model and the greater percentage released compared to DiI which has just a positively charged region.

Finally, the effect of reducing the amount of SPA contained in the cryogels (characterized in **supplementary Figure S8**) on dye loading and release was analyzed. The inclusion of lower amounts of SPA generally resulted in lower dye uptake and quicker release, with charge-neutral PEGDA alone cryogels showing that loading and release was solely due to the sponge like filling and not due to specific absorption/uptake to the cryogel structure (**supplementary Figure S9**).

3.4 Cryogel application of BODIPY to embryonic mouse brains

Embryonic mouse brains were used as a proof-of-concept that macroporous line-shaped PEGDA-co-SPA cryogels with negatively charged moieties can be used to apply a fluorescent dye to a precise area of brain tissue. The cryogels were placed directly onto the surface of dissected E14.5 mouse brains for 20 minutes (**Figure7A, B**). In addition to testing the negatively charged macroporous line-shaped PEGDA-co-SPA cryogels, we also used charge-neutral cryogels consisting of only PEGDA as a control from which to assess the biocompatibility of the SPA

functionalized cryogels (**supplementary Figure S10A**). However, they had the unexpected effect of attaching too firmly to the tissue once applied, resulting in extensive tissue damage once removed (**supplementary Figure S10A**). This was not observed with the PEGDA-co-SPA cryogels (**Figure 7C**). Instead, cross-sections through the tissue showed that the BODIPY applied to the cortical surface had penetrated the tissue and was present in the cell bodies within the cortical plate and in cell processes that extend towards the ventricular surface (**Figure 7C**). These processes belong to the progenitor cells (radial glia) and extend the entire length of the cortical wall, resulting in the band of BODIPY present at the ventricular surface (**Figure 7C**). Together this suggests that macroporous line-shaped PEGDA-co-SPA cryogels with negatively charged moieties can be successfully used to apply BODIPY to a specific region of brain tissue.

3.5 Cryogel application of BODIPY and DiI to human fetal brain slices

The macroporous line-shaped PEGDA-co-SPA cryogels were next tested in human fetal brain tissue. Two types of tissue sections were used for these tests, whole mount pieces (3D pieces, ~1-1.5 cm^3) and tissue slices (~1-1.5 cm in width and length, 2-3 mm in depth). These two types of sections were used to assess the application of dyes directly onto the surface of the tissue (whole mount pieces) or application of dyes within the tissue (tissue slices). As with the mouse tissue, macroporous line-shaped PEGDA-co-SPA cryogels loaded with BODIPY were placed directly onto the whole mount pieces of 14 weeks post-conception (pcw) human fetal brain tissue (**Figure 8A, B**) for 20 minutes.

To test the requirement of the PEGDA-co-SPA cryogels, the charge-neutral cryogels were also used with the 14 pcw human fetal brain tissue (**supplementary Figure S10B**). As with the mouse (**supplementary Figure S10A**), these charge-neutral cryogels resulted in severe damage to the tissue when they were removed, causing large tears and disruption of the tissue architecture (**supplementary Figure S10B**), indicating the need for cryogels to have the negatively charged SPA moieties. This was further tested using human fetal brain tissue that had DiI applied to the surface. The DiI was left to penetrate into the cells and then any remaining DiI was washed away before PEGDA-co-SPA cryogels and charge-neutral cryogels were placed onto the DiI-labelled area of the tissue for 2 minutes (**supplementary Figure S10C, C'**). Upon removal of the cryogels, DiI-labelled tissue had adhered to the charge-neutral cryogel, but not the PEGDA-co-SPA cryogel

(**supplementary Figure S10C, D**). This suggests that the negatively charged SPA moieties may protect against tissue damage by reducing tissue adherence to the cryogels.

Alongside BODIPY, macroporous line-shaped PEGDA-co-SPA cryogels loaded with DiI were also used alone and in combination with cryogels loaded with BODIPY (**Figure 8A**). The cryogels successfully labeled distinct and specific regions of the tissue with both different fluorescent dyes (**Figure 8A**). The BODIPY and DiI loaded cryogels were also placed directly onto the cut surface (cross-section through the cortical wall) of 17 pcw human fetal brain tissue slices to label areas within the tissue cross-sections (**Figure 8C-E**). As with the whole mount pieces (**Figure 8A**), the cryogels were also successful in labeling distinct and specific areas of the tissue slice in both a horizontal (**Figure 8D**) and vertical orientation (**Figure 8E**).

3.6 Analysis of cryogel-applied and directly-applied BODIPY surface area to human fetal brain tissue

In order to determine the spatial control of the cryogel application of BODIPY to the tissue, we measured the surface area of BODIPY on human fetal brain tissue after either cryogel application of 2.7 µl of BODIPY applied directly to the tissue (by pipette) or 2.7 µl of BODIPY loaded into a PEGDA-co-SPA cryogel and then applied to the tissue (**supplementary Figure S11A**). The surface area of BODIPY application was significantly higher when 2.7 µl of BODIPY was applied directly compared to the cryogel (**supplementary Figure S11B**), resulting in over double the surface area being labelled at either 10 or 20 minutes post-application (**supplementary Figure S11B**). In addition, we also observed that the area labelled by BODIPY was difficult to control when it was directly applied to the tissue, resulting in an almost random shape in comparison to the line of BODIPY labelling resulting from the cryogel application (**supplementary Figure S11A**).

3.7 Analysis of cryogel-applied and directly-applied BODIPY penetration into human fetal brain tissue

In addition to using the cryogels to label the surface of the tissue pieces or slices, they could also be used to label cells deeper within the tissue. To evaluate this, the depth of penetration of cryogel-applied BODIPY was measured in cross-sections taken from 12-20 pcw human fetal brain whole mount pieces and tissue slices (**Figure 9**). Cryogels were placed in different

positions directly on the cut surface of tissue slices (**Figure 9A, B**) or directly onto the surface of whole mount tissue pieces (**Figure 9A, C**). Cross-sections of this tissue were then used to assess the depth of cryogel-applied BODIPY penetration into the tissue after 10 and 20 minutes of application (**Figure 9B-D**). This analysis showed a significant increase in the depth of BODIPY penetration from 10 to 20 minutes (**Figure 9D**).

However, this was not the case when BODIPY was applied directly to the tissue (**supplementary Figure S11C, D**). In comparison to the cryogel application, directly-applied BODIPY resulted in a wider variation of depth of BODIPY penetration and no significant difference between 10 and 20 minutes of application (**supplementary Figure S11C, D**). Together, this indicates that the length of time the cryogel is applied to the tissue will alter the depth of dye penetration within the tissue, and therefore the depth at which cells can be labelled.

3.8 PEGDA-co-SPA based line-shaped cryogels load and release tetrodotoxin (TTX)

Prior to testing the feasibility of using the line-shaped cryogels to apply TTX to brain tissue slices, loading of TTX to the cryogels and the subsequent release was analyzed using PEGDA-co-SPA cryogels in comparison to charge-neutral PEGDA cryogels (**Figure 10A, C**). TTX is a monobasic acid, which presents highly ionizable groups, the potentially positively charged 7,8,9-guanidinium functionality and the C_{10}-hydroxyl group of the carboxyl side chain[48]. Once protonated, these groups can interplay via strong electrostatic interactions with negatively charged groups, such as the sulfonate groups on the PEGDA-co-SPA cryogel lines. The guanidinium group in TTX has a pK_a value of 8.76, and thus is protonated at physiological pH or even below[48]. However, the presence of the negatively charged carboxyl group with a lower pK_a value of 3.35[48] means that TTX exhibits zwitterionic character at physiological pH. Therefore, we hypothesized that the loading and release characteristics of TTX to the cryogel lines may be similar to those of BODIPY. We observed a small reduction in the TTX loading stock solution concentration for PEGDA-co-SPA cryogels which did not occur in PEGDA cryogels, (**Figure 10B, D).** This indicates that TTX is primarily taken up into the pores of the cryogel, but that electrostatic loading to the cryogel struts is also occurring when using the PEGDA-co-SPA cryogels. We hypothesize that this effect also causes the slightly reduced rate of TTX release from the PEGDA-co-SPA cryogels (**Figure 10E-G**). The cryogel width had no effect on the release kinetics (**Figure 10E-G).**

3.9 Temporal application of TTX to mouse brain tissue using cryogels

A major advantage of the PEGDA-co-SPA cryogels is the ability to remove them from the tissue, resulting in both a spatially and temporally regulated application of a compound to that area. To test the functionality of this feature, we set out to determine whether cryogels loaded with the sodium channel blocker TTX would be able to locally and reversibly inhibit neuronal action potential firing in brain tissue. Neuronal firing results in opening of voltage gated calcium channels and calcium influx. These changes in calcium concentration can be assessed using calcium indicator dyes as a proxy for neuronal activity levels in living, *ex vivo* acute brain slices[46]. Postnatal day 5-7 mouse brain slices were loaded with the calcium indicator dye Oregon Green 488 BAPTA-1 AM and control or TTX-loaded cryogels applied directly to the surface of the slice. No change in fluorescence was seen following application of control cryogels (**Figure 11A-C**), confirming that the cryogel alone did not affect activity levels. However, application of TTX-loaded cryogels resulted in a clear decrease in activity levels, which recovered back to pre-application levels during washout of TTX (**Figure 11A-C**). Following washout, the experiment was repeated with similar results (**Figure 11A, B, D**), demonstrating the reversibility of inhibition. This shows that PEGDA-co-SPA cryogels can be used to apply a pharmacological agent to a brain tissue slice that can specifically alter the function of neurons in a temporally and spatially controlled manner.

4. Discussion

In conclusion, we have developed completely synthetic, line-shaped microscale cryogels composed of PEGDA and the sulfonated monomer SPA as a novel tool for focal and reproducible labelling of human tissue explants. These materials offer several advantages: i) a user-friendly design, due to mechanical robustness and sponge-like nature ii) ease of storage prior to use iii) easy loading directly to the dry materials and controlled release of agents, and iv) precise and reproducible targeting of defined areas within tissue explants. The line-shaped cryogels were easily synthesized within well-defined PDMS molds featuring line-shaped cavities with a hydrophilic surface. The use of micro-stereolithography 3D printing to design customized micron-sized master structures provides a versatile method to adjust cryogel shapes with high definition and reproducibility.

Whilst the goal of this work was to create user-friendly tools for *ex-vivo* tissue manipulation, we speculate that the aforementioned advantages of these cryogels may extend their applications to

other research areas. The ability to manipulate a focal region of tissue would also be highly applicable for other 3D cell culture platforms, such as spheroids and organoids. This would enable researchers to have finer spatial and temporal control over the application of pharmacological agents in these cultures, enabling them to address questions that are currently difficult.
Additionally, the mechanical properties of these cryogels mean they have a high potential for the local and regional delivery of therapeutics into the *in vivo* brain[16]. The cryogels soft yet robust nature may enable them to be easily applied and removed from the brain *in vivo*, as we have demonstrated *ex vivo*. Coupled with their potential for sustained drug release, this would allow them to overcome the drawbacks of the more commonly tested polymer wafers, which suffer a mismatch in mechanical properties with the surrounding brain tissue and unfavorable burst release profiles[49].

There are many uses for a controlled and direct drug delivery to the brain, which would overcome issues arising from the impermeability of the blood brain barrier. These include the treatment of traumatic brain injury, for which silk biofilms are currently being tested in mouse models[50], or targeting the nigrostriatal pathway affected by Parkinson's Disease[51], both of which would require local drug delivery to a specific region of the brain. As well as their potential use for targeted treatments, cryogels could also be used to improve models of focal injuries themselves. Indeed, our group has recently shown that cryogels can be used as a tool to create focal demyelination of grey matter in mouse organotypic slice cultures[52] and *in vivo*[53], providing a platform technology for both mechanistic studies and to test remyelination therapeutics for Multiple-Sclerosis. Where direct injection into the brain is required, alternative templates for cryogel synthesis would probably be favorable, such as emulsion templated spherical macroporous microcarriers[54]. The cryogels developed here were designed as a simple-to-use technique for regional delivery to *ex-vivo* brain slices to address the lack of tools available for focally manipulating brain tissue in slice cultures. However, with further development they could be modified for the *in vivo* uses mentioned above, greatly widening their potential impact and applications.

The fluorescent dyes BODIPY and DiI were successfully loaded to the pores and struts of the macroporous cryogel lines and released without an initial burst. *In silico* analysis indicates that this was achieved via strong electrostatic attraction between the fluorophores and the incorporated sulfonated functionalities within the cryogels. Furthermore, the sodium channel blocker TTX could

also be loaded to the line-shaped cryogels. BODIPY, DiI and TTX were all absorbed out of the loading solutions onto SPA-containing cryogels which was not the case for charge-neutral PEGDA cryogels (where no drop in the loading solution concentration was observed). The SPA monomer was chosen for its highly acidic and negatively charged sulfonate group functionality (pK_a = -1.9)[55–57] and thus the stability of the conjugated base. This stability arises due to a spreading of the negative charge over several electronegative elements, in this case, three oxygen atoms. This charge delocalization makes it a very strong acidic component in comparison to carboxylated (R-CO_2H, $pK_a \approx 5$)[57,58] or phosphonated (R-$PO(OH)_2$, $pK_{a1} = 2.39$ and $pK_{a2} = 7.49$)[57,59] monomers that could be used as alternatives to bind ligand molecules such as dyes, drugs or proteins. Generally, such charge alterations in cryogel composition greatly improve the affinity and ligand stability[39,60,61].

This controlled release of low amounts of dyes from the PEGDA-co-SPA cryogels at their contact area with tissue allowed us to label specific regions of brain tissue without uncontrolled spreading of dye over the tissue. Moreover, the negatively charged sulfonate groups potentially caused a repulsion between the tissue membrane and the cryogel itself. We hypothesize that this may be the reason why the PEGDA-co-SPA cryogels did not result in tissue damage in contrast to the charge-neutral PEGDA control cryogels. We speculate that the charge-neutral PEGDA cryogels may form hydrogen bonds between the carbonyl functionalities, the fluorophores and the membrane surface, thus causing damage when removed from the tissue. Therefore, we do not recommend the use of cryogels made of PEGDA alone for delivery applications to live tissue cultures, even when the direct tissue contact is only of short duration.

A major advantage of using cryogels generated in PDMS templates is that this ensures equal dimensions for each cryogel and therefore targeting the same area of tissue when used for dye application. Another benefit of such line-shaped cryogels arises through their rectangular cross-section geometry which ensures a large contact surface area with the tissue. Furthermore, their flexibility and toughness allow them to snugly orientate around tissue without gaps or folds. This is especially important for use with primary human tissue, which may vary greatly in size and shape. The depth of tissue targeted can also be easily controlled by the length of time the cryogel is applied to the tissue. Currently, we have few genetic tools for this type of tissue and it can only

be manipulated by applying a substance manually, resulting in a large degree of human error[62] or the use of highly specialized equipment[63]. Additionally, these cryogels can be easily applied and removed from the tissue multiple times, allowing not only spatial control of a manipulation, but also temporal control, an important feature for functional manipulations, such as the temporary inhibition of neuronal activity by application of TTX. This novel cryogel tool will overcome these drawbacks and enable easy focal targeting of defined areas of tissue within an explant or slice culture in a user-friendly manner.

5. Conclusions

Overall, we have developed a novel biomaterial-based tool that can be used to manipulate tissue explant cultures in a precise and reproducible manner with both spatial and temporal control. These cryogels have great potential to be modified and used to deliver a wide variety of reagents to primary tissue, allowing efficient and timely manipulation of cellular function. In particular, the efficient and reversible electrostatic loading/release paradigm transforms these synthetically sulfonated line-shaped microcryogels into a useful, biocompatible, and easy-to-handle tool to control reagent delivery. Both the degree of sulfonation and the presence of other charged groups could be adapted for specific cargos, such as pharmacological inhibitors or recombinant proteins. These cryogels are of particular interest for researchers working with ex vivo model systems where genetic tools are lacking, such as primary human tissue, but could be also applied in many different fields.

Acknowledgments

The authors would like to thank the following funding sources: Wellcome Trust (Sir Henry Wellcome Postdoctoral Fellowship (BN)), the Deutsche Forschungsgemeinschaft (project number 320041273) and the Medical Research Council [MR/S025065/1] (KL). JT receives funding from the European Research Council (ERC) under the European Union's Horizon 2020 research and innovation program (Grant agreement No. 852065). We would also like to thank Dianne Gerrelli, Steve Lisgo, Berta Crespo, and their teams at the HDBR for their invaluable support.

Competing Interests:

The authors declare that they have no competing interests.

Data Availability:

Supplementary Information: Supplementary Figures S1-S11 and videos V1-4.

References

1. Lancaster, M. A. *et al.* Cerebral organoids model human brain development and microcephaly. *Nature* **501**, 373–9 (2013).
2. Mason, J. O. & Price, D. J. Building brains in a dish: Prospects for growing cerebral organoids from stem cells. *Neuroscience* **334**, 105–118 (2016).
3. Lancaster, M. A. & Huch, M. Disease modelling in human organoids. *Dis. Model. Mech.* **12**, dmm039347 (2019).
4. Di Lullo, E. & Kriegstein, A. R. The use of brain organoids to investigate neural development and disease. *Nat. Rev. Neurosci.* **18**, 573–584 (2017).
5. Ardhanareeswaran, K., Mariani, J., Coppola, G., Abyzov, A. & Vaccarino, F. M. Human induced pluripotent stem cells for modelling neurodevelopmental disorders. *Nat. Rev. Neurol.* (2017). doi:10.1038/nrneurol.2017.45
6. Kyrousi, C. & Cappello, S. Using brain organoids to study human neurodevelopment, evolution and disease. *Wiley Interdiscip. Rev. Dev. Biol.* e347 (2019). doi:10.1002/wdev.347
7. Molnár, Z. *et al.* New insights into the development of the human cerebral cortex. *J. Anat.* joa.13055 (2019). doi:10.1111/joa.13055
8. Camp, J. G. *et al.* Human cerebral organoids recapitulate gene expression programs of fetal neocortex development. *Proc. Natl. Acad. Sci. U. S. A.* **112**, 15672–7 (2015).
9. Seto, Y. & Eiraku, M. Human brain development and its in vitro recapitulation. *Neurosci. Res.* **138**, 33–42 (2019).
10. Johnson, M. B. *et al.* Single-cell analysis reveals transcriptional heterogeneity of neural progenitors in human cortex. *Nat. Neurosci.* (2015). doi:10.1038/nn.3980
11. Pollen, A. A. *et al.* Molecular Identity of Human Outer Radial Glia during Cortical Development. *Cell* **163**, 55–67 (2015).
12. Mayer, S. *et al.* Multimodal Single-Cell Analysis Reveals Physiological Maturation in the Developing Human Neocortex. *Neuron* **102**, 143-158.e7 (2019).
13. Darmanis, S. *et al.* A survey of human brain transcriptome diversity at the single cell level. *Proc. Natl. Acad. Sci. U. S. A.* **112**, 7285–7290 (2015).
14. Fan, X. *et al.* Spatial transcriptomic survey of human embryonic cerebral cortex by single-cell RNA-seq analysis. *Cell Res.* **28**, 730–745 (2018).
15. Burdick, J. A., Ward, M., Liang, E., Young, M. J. & Langer, R. Stimulation of neurite outgrowth by neurotrophins delivered from degradable hydrogels. *Biomaterials* **27**, 452–459 (2006).
16. Bastiancich, C., Danhier, P., Préat, V. & Danhier, F. Anticancer drug-loaded hydrogels as drug delivery systems for the local treatment of glioblastoma. *Journal of Controlled Release* **243**, 29–42 (2016).
17. Pakulska, M. M., Vulic, K., Tam, R. Y. & Shoichet, M. S. Hybrid crosslinked methylcellulose hydrogel: A predictable and tunable platform for local drug delivery. *Adv. Mater.* **27**, 5002–5008 (2015).
18. Tuladhar, A. *et al.* Injectable hydrogel enables local and sustained co-delivery to the brain: Two clinically approved biomolecules, cyclosporine and erythropoietin, accelerate functional recovery in rat model of stroke. *Biomaterials* **235**, (2020).
19. Lozinsky, V. Cryostructuring of Polymeric Systems. 50.† Cryogels and Cryotropic Gel-

Formation: Terms and Definitions. *Gels* **4**, 77 (2018).
20. Kirsebom, H., Rata, G., Topgaard, D., Mattiasson, B. & Galaev, I. Y. Mechanism of cryopolymerization: Diffusion-controlled polymerization in a nonfrozen microphase. An NMR study. *Macromolecules* **42**, 5208–5214 (2009).
21. Kirsebom, H., Topgaard, D., Galaev, I. Y. & Mattiasson, B. Modulating the porosity of cryogels by influencing the nonfrozen liquid phase through the addition of inert solutes. *Langmuir* **26**, 16129–16133 (2010).
22. Mehdi Razavi, Sophia Hu, and A. S. T. A collagen based cryogel bioscaffold coated with nanostructured polydopamine as a platform for mesenchymal stem cell therapy. *Physiol. Behav.* **106**, 2213–2228 (2018).
23. Bakhshpour, M., Idil, N., Perçin, I. & Denizli, A. Biomedical applications of polymeric cryogels. *Appl. Sci.* **9**, 1–22 (2019).
24. Memic, A. *et al.* Latest Advances in Cryogel Technology for Biomedical Applications. *Adv. Ther.* **2**, 1800114 (2019).
25. Lozinsky, V. I. *et al.* Cryostructuring of polymer systems. XXIX. Preparation and characterization of supermacroporous (spongy) agarose-based cryogels used as three-dimensional scaffolds for culturing insulin-producing cell aggregates. *J. Appl. Polym. Sci.* **108**, 3046–3062 (2008).
26. Bhat, S., Tripathi, A. & Kumar, A. Supermacroprous chitosan-agarose-gelatin cryogels: In vitro characterization and in vivo assessment for cartilage tissue engineering. *J. R. Soc. Interface* **8**, 540–554 (2011).
27. Kumari, J. & Kumar, A. Development of polymer based cryogel matrix for transportation and storage of mammalian cells. *Sci. Rep.* **7**, 1–13 (2017).
28. Newland, B. *et al.* Macroporous heparin-based microcarriers allow long-term 3D culture and differentiation of neural precursor cells. *Biomaterials* **230**, (2020).
29. Newland, B. *et al.* Tackling cell transplantation anoikis: An injectable, shape memory cryogel microcarrier platform material for stem cell and neuronal cell growth. *Small* **11**, 5047–5053 (2015).
30. Eggermont, L. J., Rogers, Z. J., Colombani, T., Memic, A. & Bencherif, S. A. Injectable cryogels for biomedical applications. *Trends in Biotechnology* **38**, 418–431 (2020).
31. Welzel, P. B. *et al.* Macroporous starPEG-heparin cryogels. *Biomacromolecules* **13**, 2349–2358 (2012).
32. Sargeant, T. D., Desai, A. P., Banerjee, S., Agawu, A. & Stopek, J. B. An in situ forming collagen-PEG hydrogel for tissue regeneration. *Acta Biomater.* **8**, 124–132 (2012).
33. Dekosky, B. J. *et al.* Hierarchically designed agarose and poly(ethylene glycol) interpenetrating network hydrogels for cartilage tissue engineering. *Tissue Eng. - Part C Methods* **16**, 1533–1542 (2010).
34. Wu, J., Zhao, Q., Sun, J. & Zhou, Q. Preparation of poly(ethylene glycol) aligned porous cryogels using a unidirectional freezing technique. *Soft Matter* **8**, 3620–3626 (2012).
35. Hwang, Y., Zhang, C. & Varghese, S. Poly(ethylene glycol) cryogels as potential cell scaffolds: Effect of polymerization conditions on cryogel microstructure and properties. *J. Mater. Chem.* **20**, 345–351 (2010).
36. Dispinar, T., Van Camp, W., De Cock, L. J., De Geest, B. G. & Du Prez, F. E. Redox-responsive degradable PEG cryogels as potential cell scaffolds in tissue engineering. *Macromol. Biosci.* **12**, 383–394 (2012).
37. Wu, J. *et al.* Sulfated zwitterionic poly(sulfobetaine methacrylate) hydrogels promote complete skin regeneration. *Acta Biomater.* **71**, 293–305 (2018).
38. Bernards, S. L. H. and M. T. Polyampholyte hydrogels in biomedical applications. *Gels* **3**,

41 (2017).
39. Saparov, A. *et al.* Composite cryogel with polyelectrolyte complexes for growth factor delivery. *Pharmaceutics* **11**, 1–15 (2019).
40. Kudaibergenov, S. E. Physicochemical, complexation and catalytic properties of polyampholyte cryogels. *Gels* **5**, (2019).
41. Mastropietro, D. J., Omidian, H. & Park, K. Drug delivery applications for superporous hydrogels. *Expert Opinion on Drug Delivery* **9**, 71–89 (2012).
42. Omidian, H., Park, K. & Rocca, J. G. Recent developments in superporous hydrogels. *J. Pharm. Pharmacol.* **59**, 317–327 (2007).
43. Woodward, R. B. The structure of tetrodotoxin. *Pure Appl. Chem.* **9**, 49–74 (1964).
44. Noguchi, T. & Mahmud, Y. Current methodologies for detection of tetrodotoxin. *Journal of Toxicology - Toxin Reviews* **20**, 35–50 (2001).
45. Grillo, F. W. *et al.* A distance-dependent distribution of presynaptic boutons tunes frequency-dependent dendritic integration. *Neuron* **99**, 275-282.e3 (2018).
46. Dawitz, J., Kroon, T., Johannes Hjorth, J. J. & Meredith, R. M. Functional calcium imaging in developing cortical networks. *J. Vis. Exp.* 3550 (2011). doi:10.3791/3550
47. Long, K. R. *et al.* Extracellular matrix components HAPLN1, lumican, and collagen I cause hyaluronic acid-dependent folding of the developing human neocortex. *Neuron* **99**, 702-719.e7 (2018).
48. Goto, T., Kishi, Y., Takahashi, S. & Hirata, Y. Further studies on the structure of tetrodotoxin. *Tetrahedron Lett.* **5**, 779–786 (1964).
49. Tabet, A. *et al.* Designing next-generation local drug delivery vehicles for glioblastoma adjuvant chemotherapy: Lessons from the clinic. *Advanced Healthcare Materials* **8**, (2019).
50. Tang-Schomer, M. D., Kaplan, D. L. & Whalen, M. J. Film interface for drug testing for delivery to cells in culture and in the brain. *Acta Biomater.* **94**, 306–319 (2019).
51. Ucar, B. *et al.* Biomaterial based strategies to reconstruct the nigrostriatal pathway in organotypic slice co-cultures. *Acta Biomater.* **121**, 250–262 (2020).
52. Eigel, D. *et al.* Cryogel scaffolds for regionally constrained delivery of lysophosphatidylcholine to central nervous system slice cultures: A model of focal demyelination for multiple sclerosis research. *Acta Biomater.* **97**, 216–229 (2019).
53. Zoupi, L. *et al.* Selective vulnerability of inhibitory networks in multiple sclerosis. *Acta Neuropathol.* **1**, 3 (2021).
54. Schirmer, L. *et al.* Heparin-based, injectable microcarriers for controlled delivery of interleukin-13 to the brain. *Biomater. Sci.* **8**, 4997–5004 (2020).
55. Nalampang, K., Panjakha, R., Molloy, R. & Tighe, B. J. Structural effects in photopolymerized sodium AMPS hydrogels crosslinked with poly(ethylene glycol) diacrylate for use as burn dressings. *J. Biomater. Sci. Polym. Ed.* **24**, 1291–1304 (2013).
56. Guthrie, J. P. Hydrolysis of esters of oxy acids: pKa values for strong acids; Brønsted relationship for attack of water at methyl; free energies of hydrolysis of esters of oxy acids; and a linear relationship between free energy of hydrolysis and pKa holding over a ran. *Can. J. Chem.* **56**, 2342–2354 (1978).
57. Elliott, T. S., Slowey, A., Ye, Y. & Conway, S. J. The use of phosphate bioisosteres in medicinal chemistry and chemical biology. *MedChemComm* **3**, 735–751 (2012).
58. Carlo, B., Donna, M. H. & Amos, B. Smith, L. Carboxylic Acid (Bio)lsosteres in Drug Design. *ChemMedChem* **8**, 385–395 (2013).
59. Doak, L. D. F. and G. O. *The preparation and properties of phosphonic acids*. (1956).
60. Saylan, Y. & Denizli, A. Supermacroporous composite cryogels in biomedical

applications. *Gels* **5**, (2019).
61. Offeddu, G. S. *et al.* Cartilage-like electrostatic stiffening of responsive cryogel scaffolds. *Sci. Rep.* **7**, 1–10 (2017).
62. Taverna, E., Haffner, C., Pepperkok, R. & Huttner, W. B. A new approach to manipulate the fate of single neural stem cells in tissue. *Nat. Neurosci.* **15**, 329–37 (2012).
63. Shull, G., Haffner, C., Huttner, W. B., Kodandaramaiah, S. B. & Taverna, E. Robotic platform for microinjection into single cells in brain tissue. *EMBO Rep.* **20**, (2019).

Figures

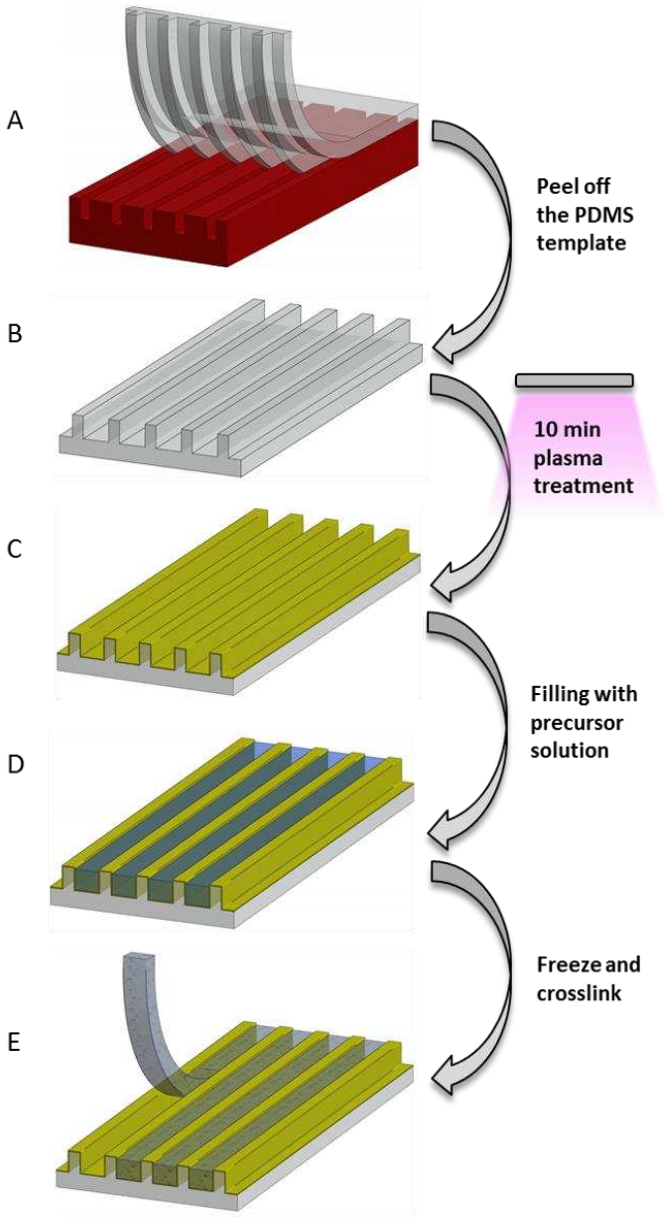

Figure (1). Schematic depiction of the line-shaped cryogel fabrication process.

(A) Fabrication of the PDMS line-shaped template, including (B) peeling off the template from the 3D printed master, (C) plasma treatment, (D) filling with precursor solution, (E) cryogelation and harvesting of the line-shaped cryogels from the template.

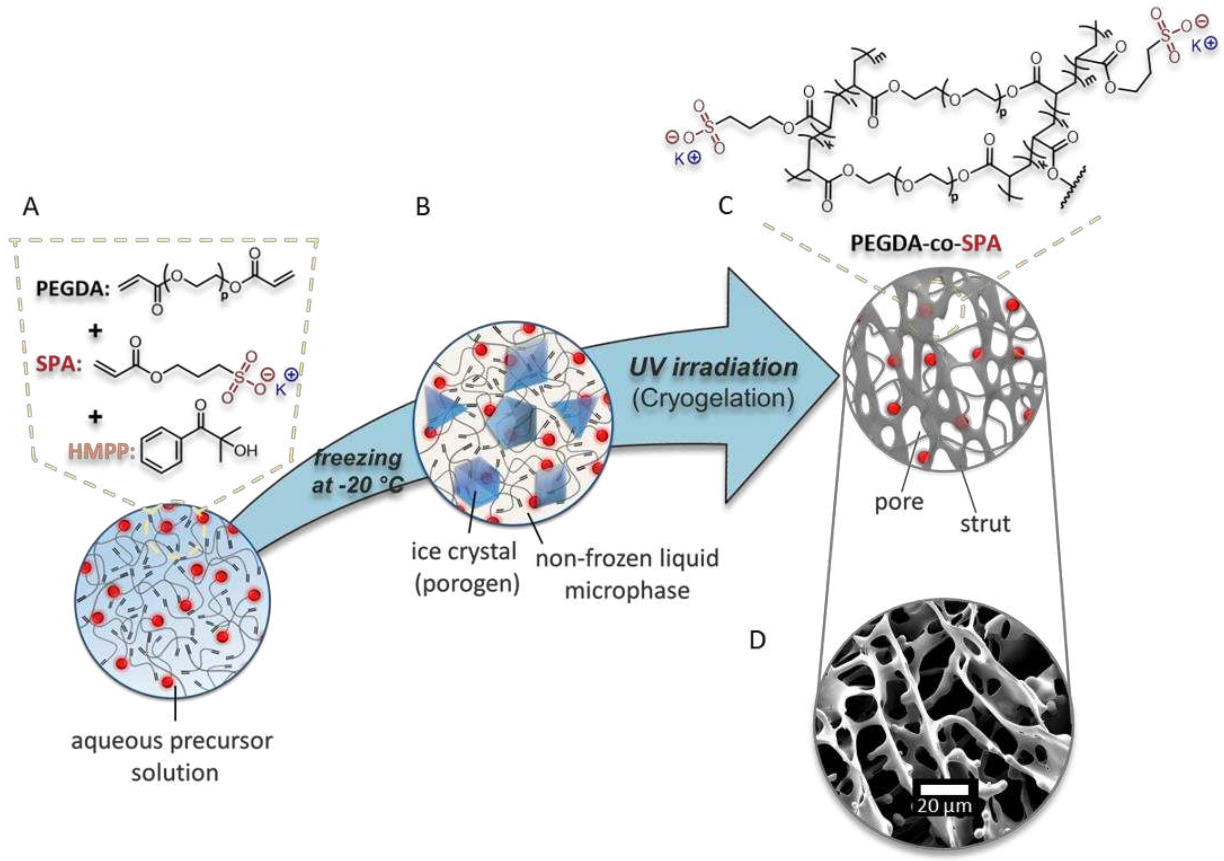

Figure (2). Schematic depiction of the PEGDA-co-SPA cryogel synthesis.

(A) Aqueous precursor solution containing PEGDA and SPA as monomers and HMPP as the photoinitiator. (B) Formation of a non-frozen liquid microphase and ice crystals due to the freezing process (cryogenic treatment). (C) Synthesis of a PEGDA-co-SPA network via UV initiated free radical photo-polymerization reaction within the liquid non-frozen microphase (cryogelation). (D) SEM image of the resulting scaffold after crosslinking, which appears as a highly porous structure.

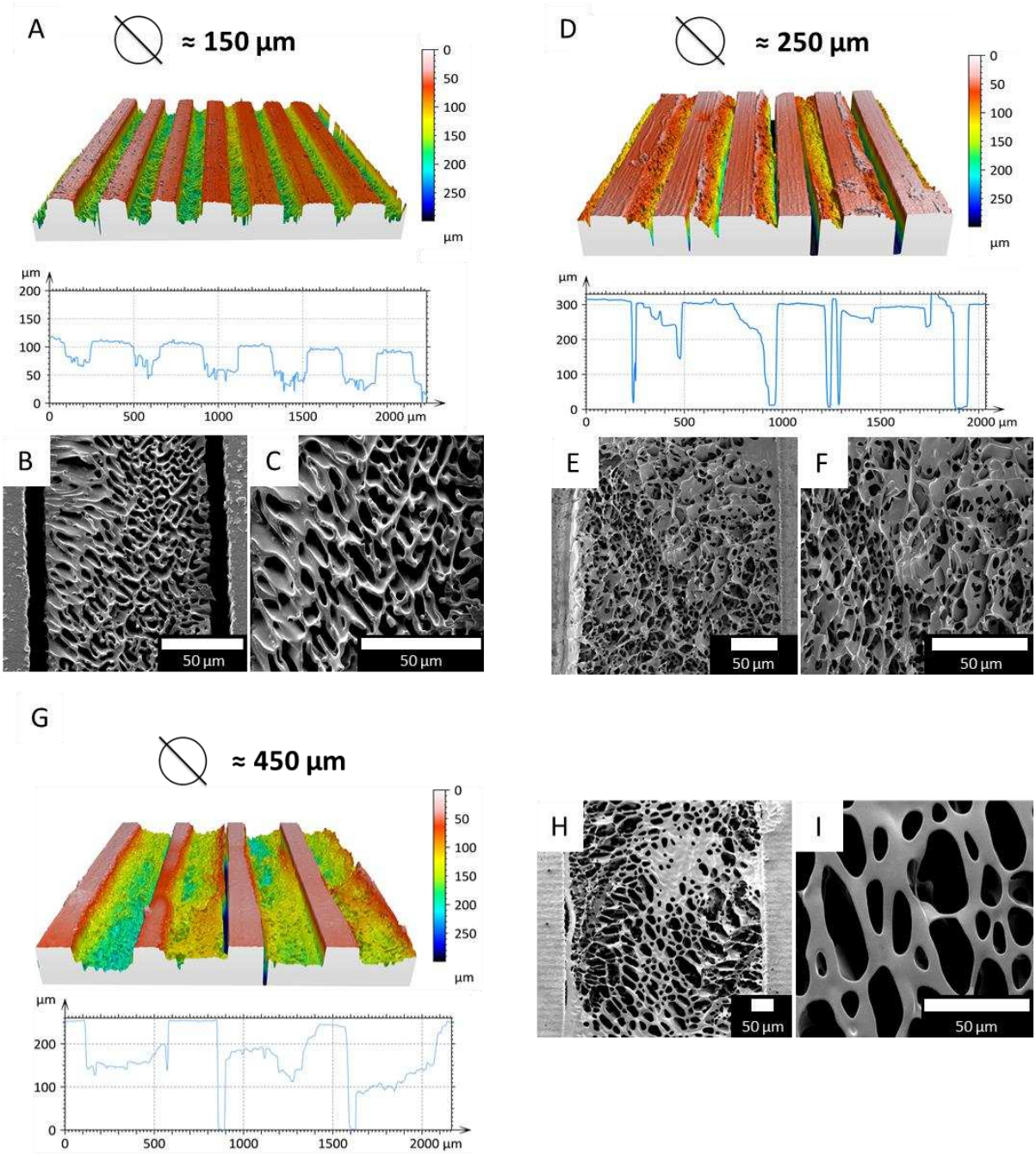

Figure (3). Characterization of the line-shaped cryogel filled templates.

Cavity dimensions of 150 µm (A-C), 250 µm (D-F), and 450 µm (G-I) were analyzed after cryogelation. 3D multi-pinhole confocal microscopy with profile section analysis (A, D, G) and scanning electron microscopy (SEM) images (B, C, E, F, H, I) show the porous nature of the line-shaped PEGDA-co-SPA scaffolds in their dehydrated state.

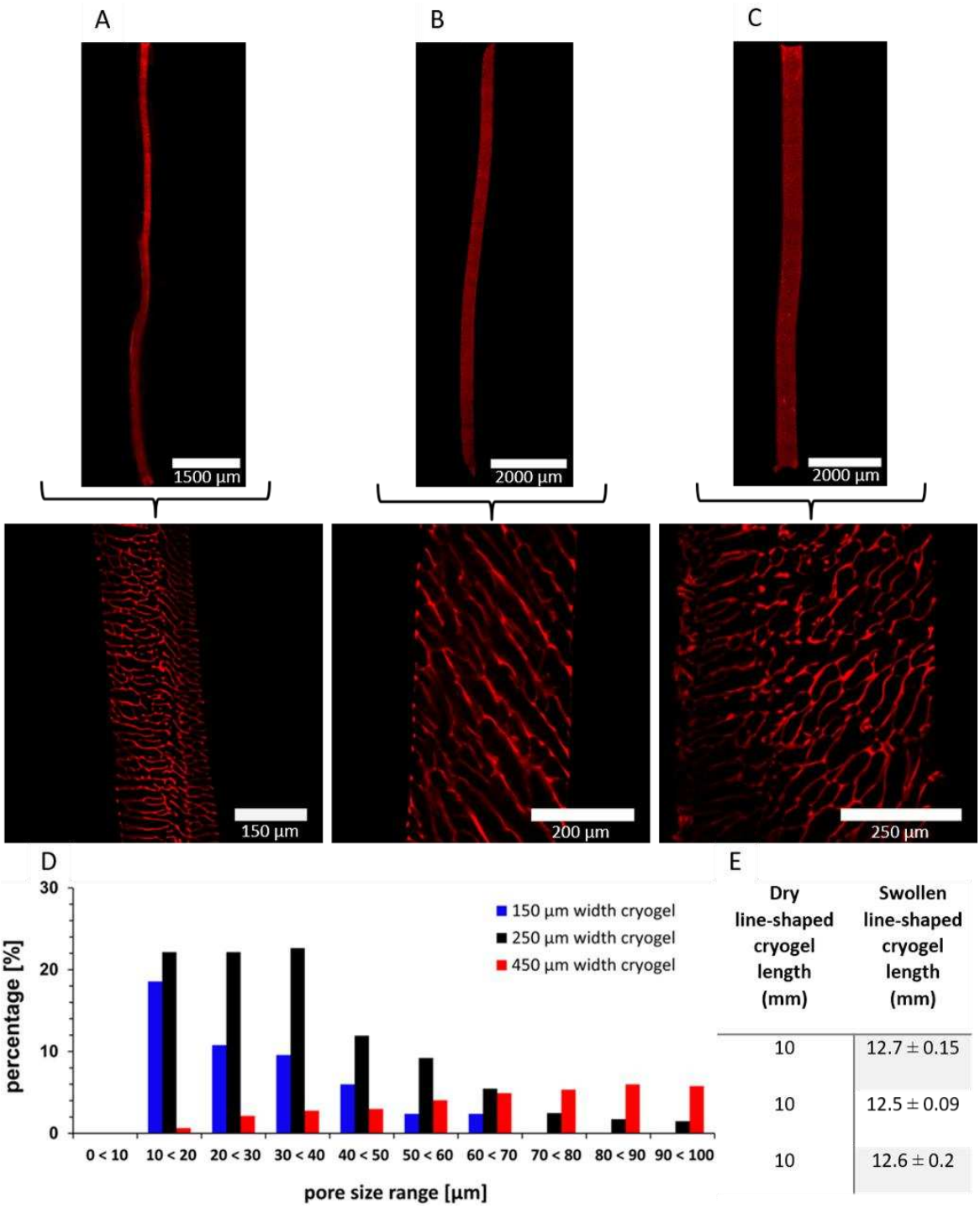

Figure (4). Confocal laser scanning fluorescence microscopy (CLSM) analysis of line-shaped PEGDA-co-SPA cryogel scaffolds.

CLSM analysis of ATTO 647 maleimide labelled line-shaped PEGDA-co-SPA cryogels in their hydrated state created from templates with widths of 150 µm (A), 250 µm (B), and 450 µm (C) showing the high precision control over scaffold dimensions and their macroporosity. (D) Pore size distribution analysis of line-shaped cryogels with widths of 150 µm, 250 µm, and 4500 µm. A

total number of 400 pores was counted for each of the differently sized line-shaped cryogels. (E) Comparison of cryogel lengths in their dry and hydrated state in PBS at 37 °C. Data collected are presented as mean ± standard deviation (n=6).

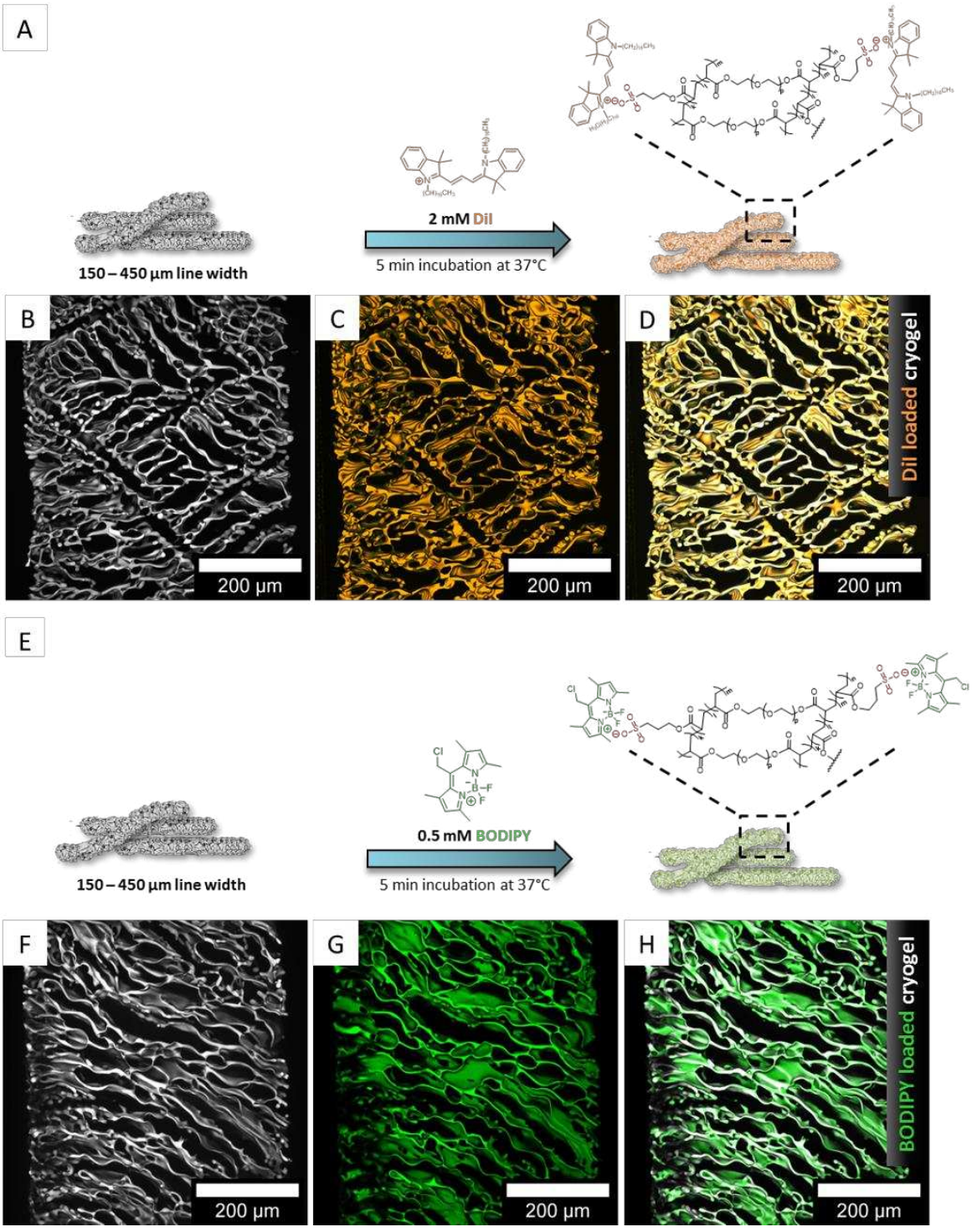

Figure (5). Confocal laser scanning fluorescence microscopy (CLSM) analysis of line-shaped PEGDA-co-SPA cryogels loaded with BODIPY and DiI.

(A,E) An illustration of the electrostatic interactions between the negatively charged sulfonate groups of the line-shaped PEGDA-co-SPA cryogels and the positively charged moieties of either DiI (nitrogen of the indoline ring within the indocarbocyanine) or BODIPY (nitrogen within the dipyrromethene ring). Representative CLSM analysis of 450 µm wide line-shaped PEGDA-co-SPA based cryogels loaded with

either DiI (B-D) or BODIPY (F-H). BODIPY and DiI appear to be quite homogeneously loaded and distributed over the cryogel structure.

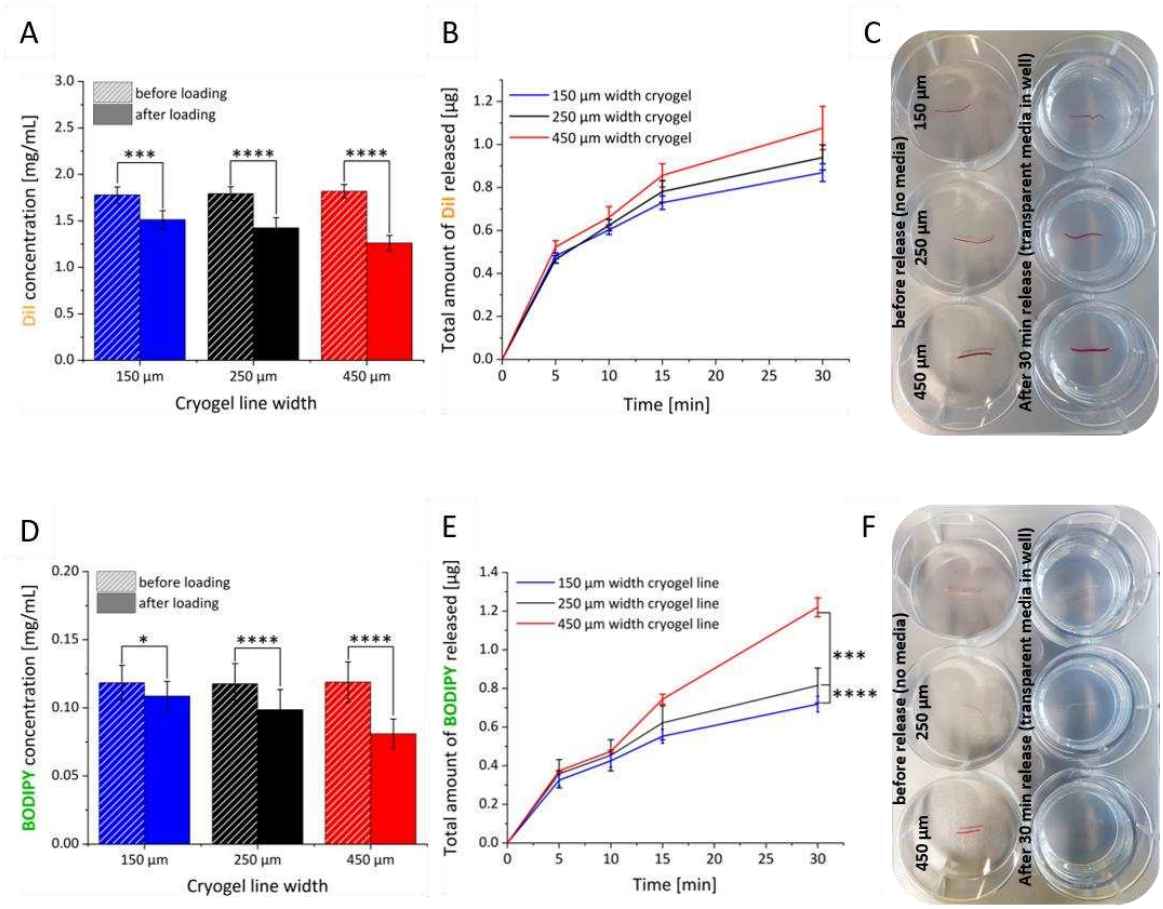

Figure (6). Loading and release properties of DiI and BODIPY from the negatively charged line-shaped PEGDA-co-SPA cryogels.

(A-C) Loading and release properties of DiI from the 150-450 µm width PEGDA-co-SPA cryogels. (A) Shows a reduction of the stock solution concentration after the loading process. The amount of dye loaded tended to increase slightly with increasing cryogel size. (B) Release profile demonstrating the very low amount of DiI delivered from the cryogels over 30 minutes. (C) DiI loaded cryogels (dark purple-red color) placed in empty 6-well inserts (left column) and imaged after 30 minutes of release in wells containing media (right column) showing that the cryogels retain their intense color. (D-F) Loading and release properties of BODIPY from the 150-450 µm widths PEGDA-co-SPA cryogels. (D) Shows a reduction of the dye concentration in the loading solution due to uptake by the cryogels. (E) A controlled-release profile was obtained with a low amount of BODIPY released from the cryogels for 30 minutes. (F) Images of BODIPY loaded cryogels in 6-well inserts in empty wells (left column) and wells containing media (right column). The dye loaded cryogels were slightly orange-red (left column) but after 30 minutes of release, the cryogels appear completely discolored (right row). Statistical analysis: Error bars represent the

cumulative value of the standard error (n = 4). Two-way ANOVA with Bonferroni´s post-hoc multiple comparisons test (∗P < 0.05, ∗∗P < 0.01, ∗∗∗P < 0.001, ∗∗∗∗P < 0.0001). Data presented as mean ± standard error including two-way ANOVA with Bonferroni´s multiple comparison test.

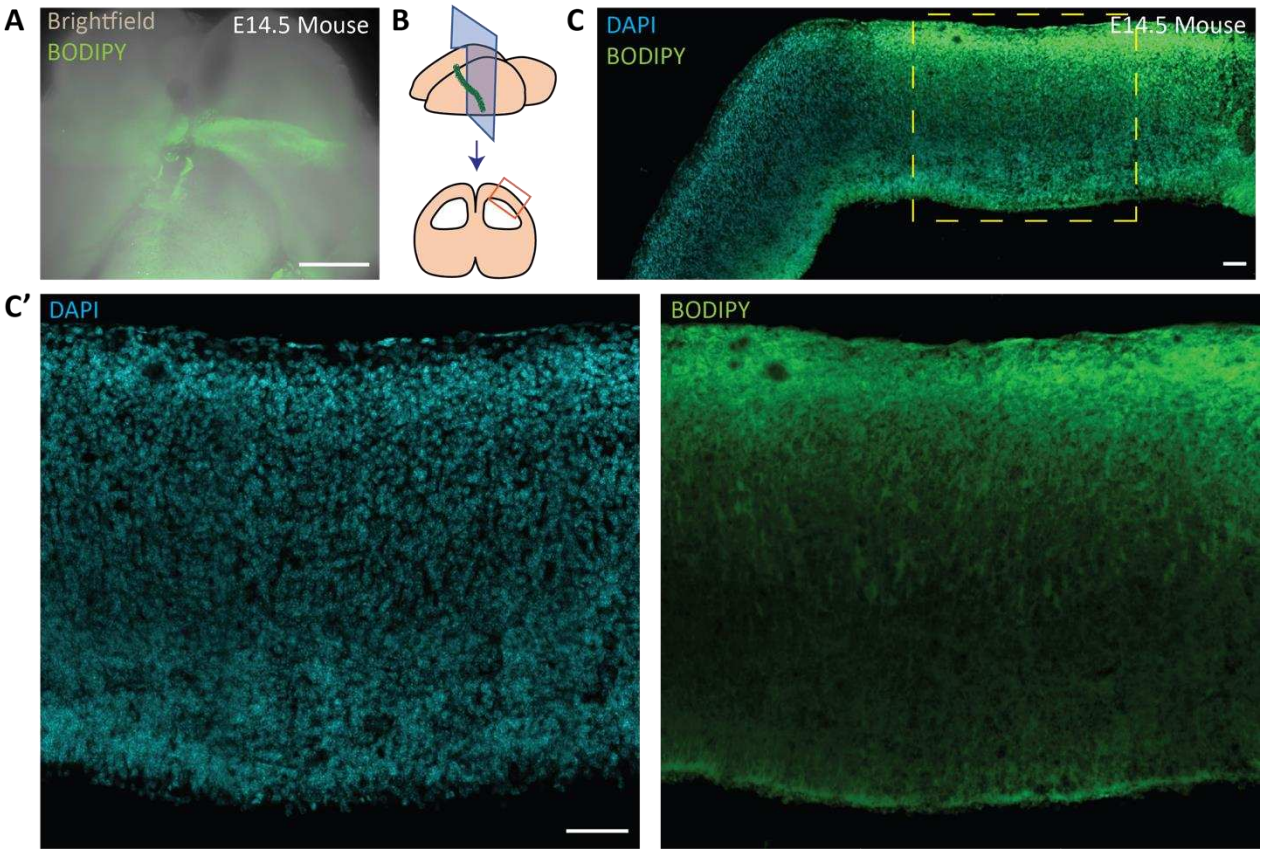

Figure (7). Application of BODIPY dye to E14.5 mouse brain using 450 µm wide line-shaped cryogels.

(A) Brightfield image of the whole E14.5 mouse brain. BODIPY was applied to the right hemisphere using a 450 µm wide line-shaped cryogel. Scale bar 1mm. (B) Schematic showing whole E14.5 mouse brain, cryogel placement, and a cross-section through it displayed in C. (C) Cross-section through E14.5 cortex where BODIPY has been applied using a 450 µm wide cryogel to the basal cortical surface (top of image). Yellow box delineates areas shown in C'. DAPI (blue) used to label the nuclei within the tissue. (C') DAPI and BODIPY within the cross-section of the cortical wall. Application of BODIPY to the basal surface (top of image) has penetrated into cells at the basal surface (neurons and basal end feet of radial glia progenitors) and stains the processes of these cells as they extend into the tissue. Scale bars 50 µm.

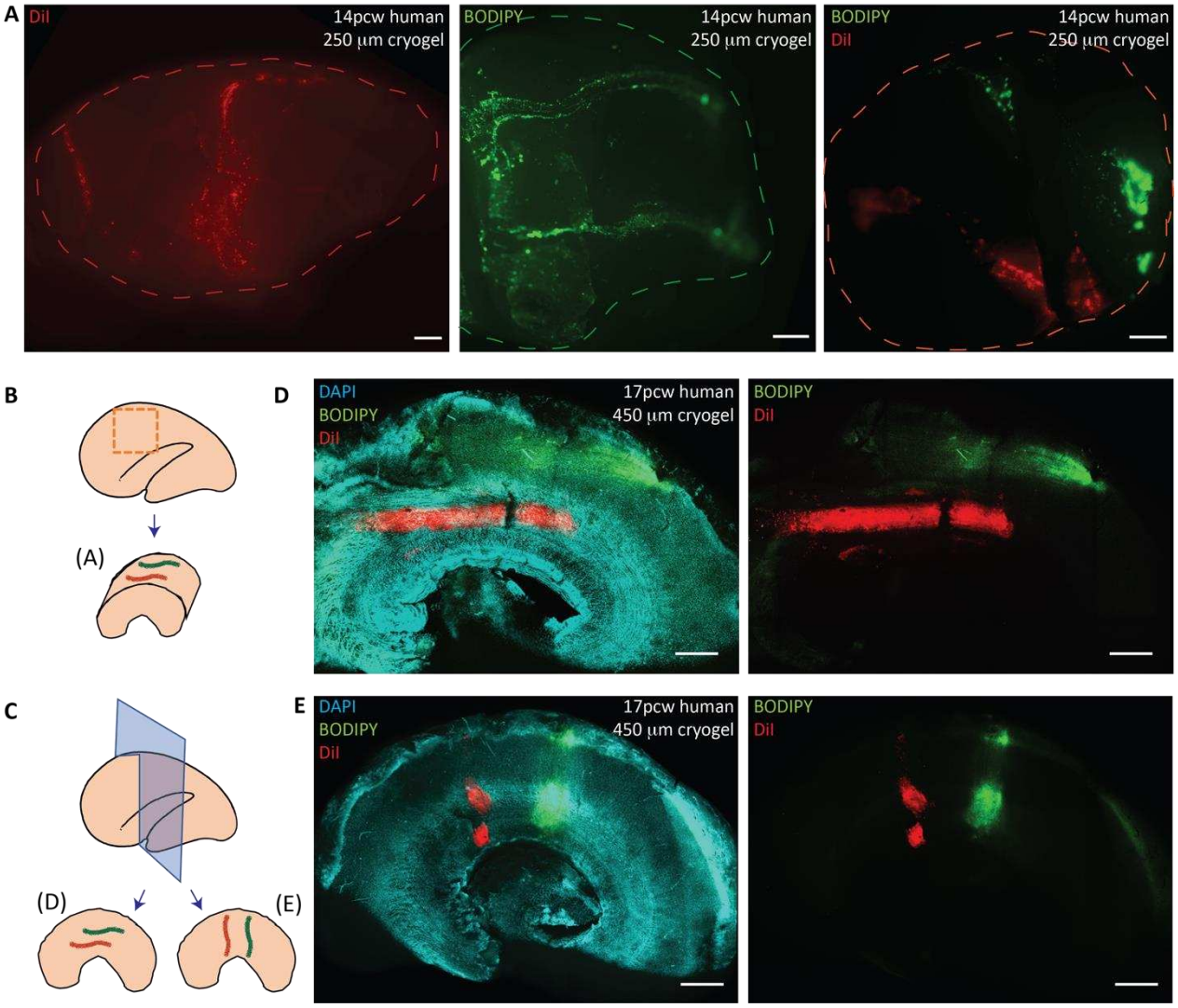

Figure (8). Application of BODIPY and DiI dyes to 14pcw and 17 pcw human fetal cortex using 250 µm and 450 µm wide line-shaped cryogels.

(A) Whole mount images of 14pcw human fetal cortex pieces. DiI, BODIPY or both dyes were applied to the tissue using 250 µm wide line-shaped cryogels. Two cryogels were applied per tissue piece. Tissue pieces are outlined by dashed lines. (B and C) Schematics showing whole fetal human brain, cryogel placement and (B) 3D section through the cortex displayed in A, and (C) cross-section through the cortex displayed in D and E. (D and E) Whole mount images of slices through 17pcw human fetal cortex pieces. DiI and BODIPY dyes were applied using 450 µm wide line-shaped cryogels. Two cryogels were applied per tissue piece. DAPI (blue) used to label the nuclei within the tissue (left panels). Cryogels were applied horizontally across the tissue, to label

progenitor zones (red) or neuronal zones (cortical plate, green) (D), or, vertically to label cortical columns (E). Scale bars 1 mm.

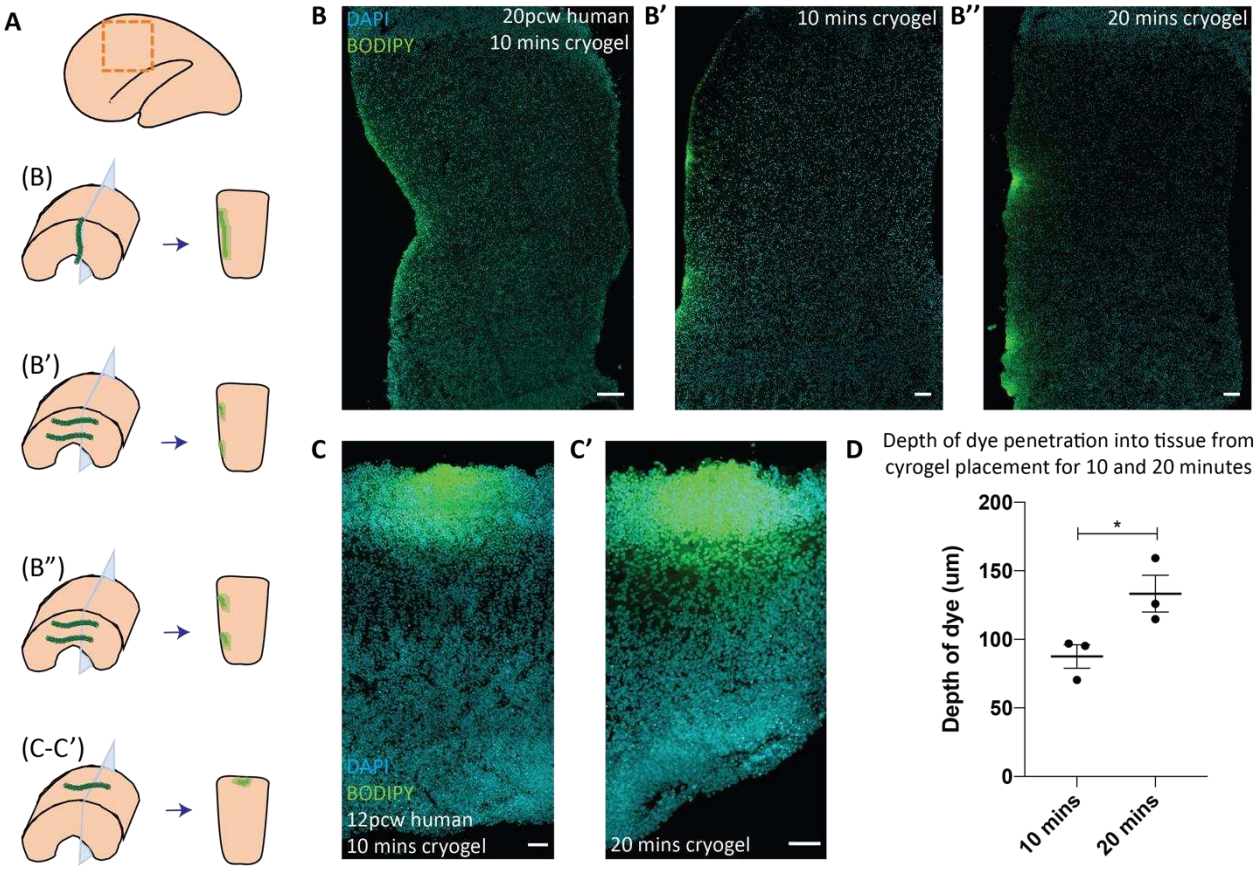

Figure (9). Application of BODIPY dye to 20pcw and 12 pcw human fetal cortex using 250 µm and 450 µm wide line-shaped cryogels.

(A) Schematics showing whole fetal human brain and 3D sections through the cortex used for B-C. Each 3D section shows the placement of cryogel and cross-section shown in the corresponding image. (B-B'') Cross-sections of 20pcw human fetal cortex pieces. BODIPY dye was applied using 250 µm and 450 µm wide line-shaped cryogels. Two cryogels were applied per tissue piece. DAPI (blue) used to label the nuclei within the tissue (left panels). (B) Cross-section showing a 250 µm wide cryogel applied vertically across the tissue showing BODIPY staining along the entire cortical wall. (B'-B'') Cross-section showing 450 µm (left) and 250 µm (right) cryogels applied horizontally across the tissue showing BODIPY in two areas of the cortical wall. Cryogels were used for 10 minutes (B') and 20 minutes (B''). Scale bars 100 µm. (C-C') Cross-sections of 12pcw human fetal cortex pieces. BODIPY dye was applied using 250 µm wide line-shaped cryogels placed on the basal surface of the cortical tissue (top of image). Images show BODIPY staining in

the cortical plate after cryogel application for 10 minutes (C) and 20 minutes (C'). Scale bars 50 µm. (D) Quantification of the depth of BODIPY penetration into the tissue after 10 and 20 minutes of application. Statistical analysis: Error bars represent standard error (n = 3). T-test, * $p = 0.045$.

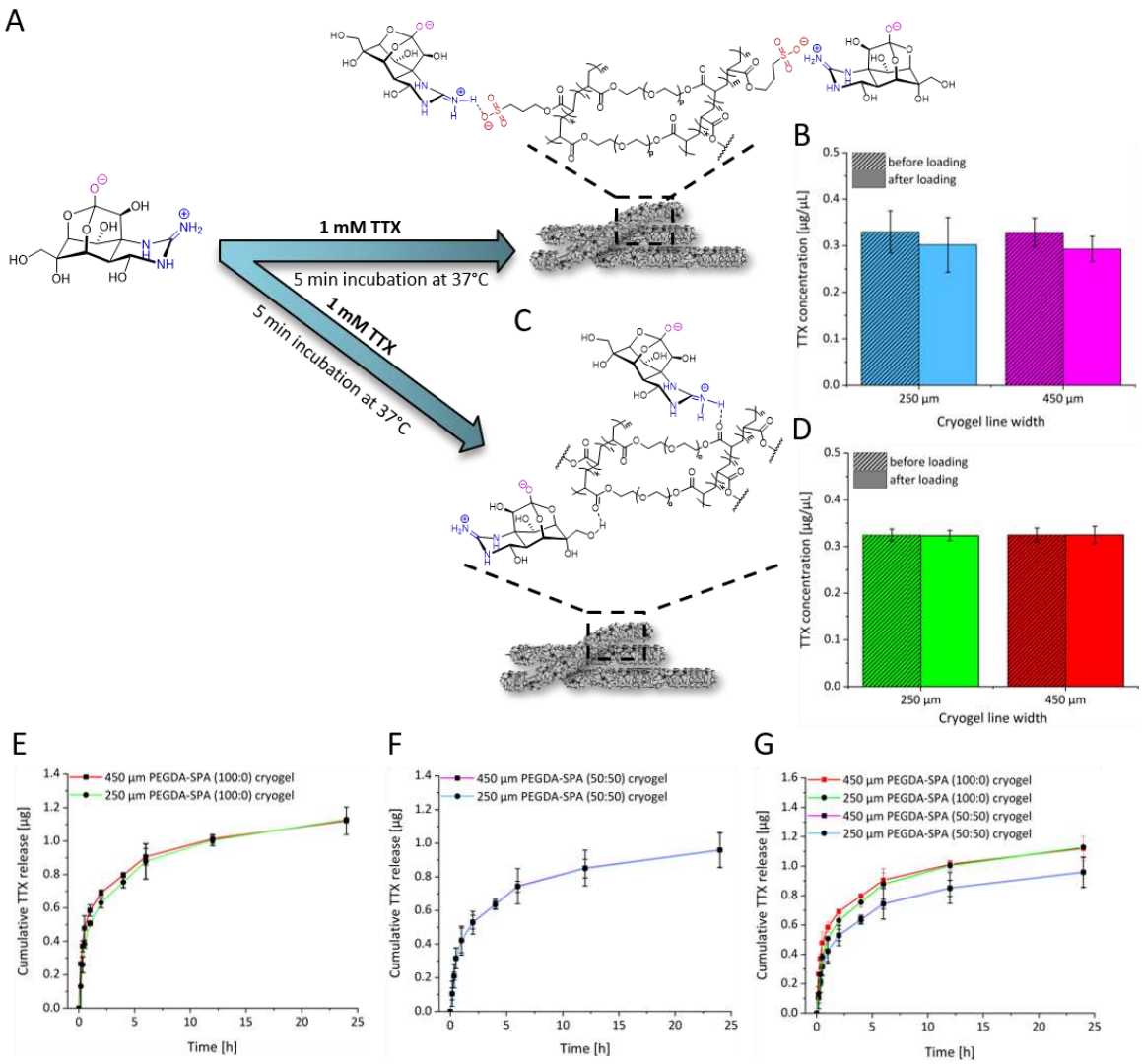

Figure (10). Loading and release properties of tetrodotoxin (TTX) from the negatively charged PEGDA-co-SPA cryogels and PEGDA alone cryogels. (A) An illustration of the electrostatic interactions between the negatively charged sulfonate groups of the line-shaped PEGDA-co-SPA cryogels and the positively charged guanidine moiety of TTX. (B) Loading properties of TTX from the 250 µm and 450 µm width PEGDA-co-SPA line-shaped cryogels with a SPA content (sulfonation degree) of 50%. After the loading process, a marginal reduction of the TTX stock solution concentration is present due to electrostatic uptake to the cryogels, which is independent of the line-shaped cryogel width. (C) An illustration of the molecular interactions between line-shaped PEGDA cryogel network without charged sulfonate groups and TTX. (D) Loading properties of TTX from the 250 µm and 450 µm width PEGDA cryogels. After the loading process, no reduction of the TTX stock solution concentration is present. (n = 3) (error bars represent ± standard deviation). (E-G) Release properties of TTX from the line-shaped

PEGDA or PEGDA-co-SPA cryogels of widths 250 µm or 450 µm. (n = 3) (error bars represent the cumulative value of the standard error).

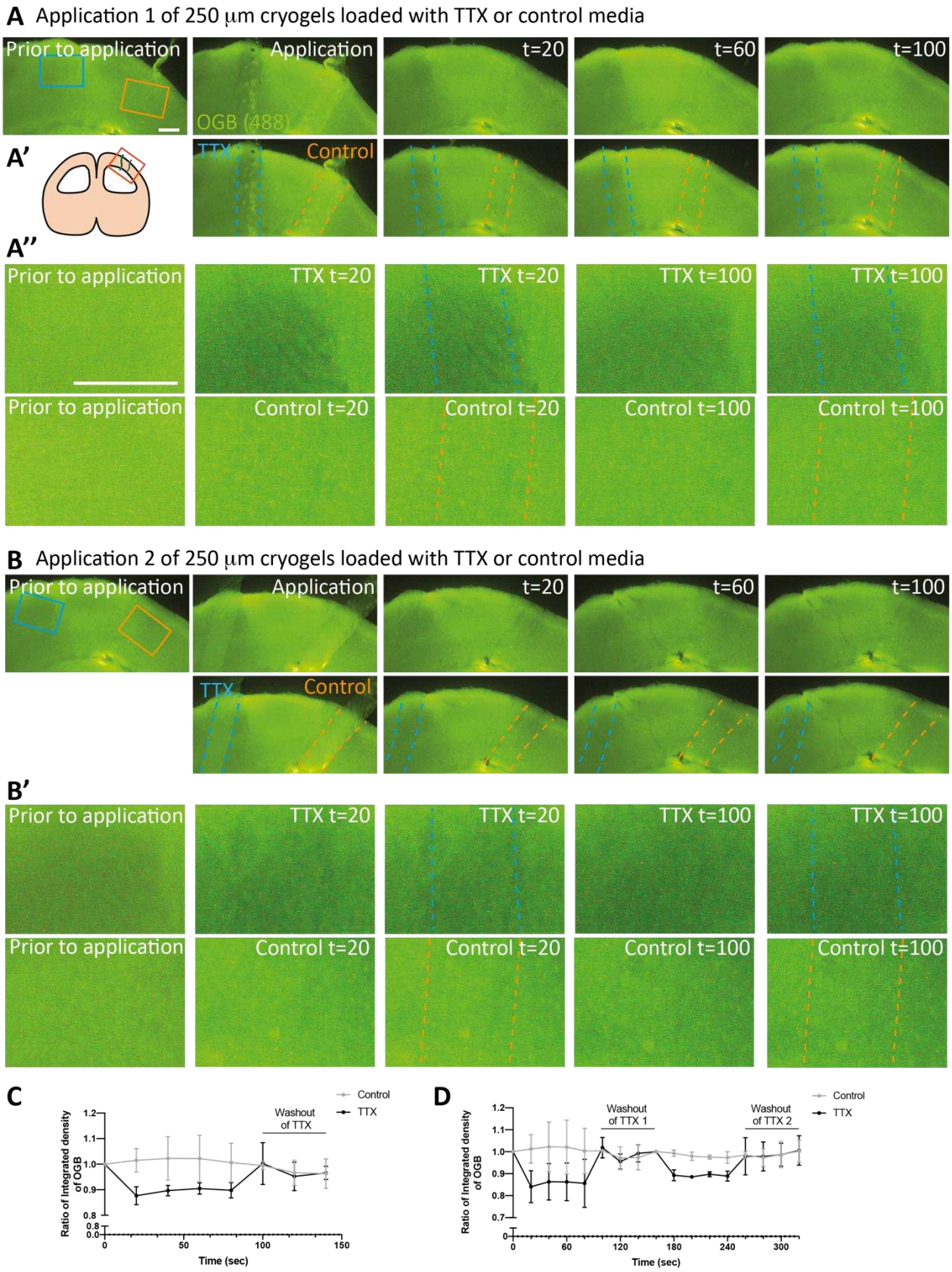

Figure (11). Application of TTX to P5-7 postnatal mouse brain tissue slices using 250 μm wide line-shaped cryogels.

(A) Whole mount images of P5 mouse cortex slice loaded with the calcium indicator fluorescent dye OGB (green). Images show the level of OGB fluorescence prior to application, the cryogel application, and then 20, 60 and 100 seconds after cryogel removal. Control cryogels and areas targeted are delineated by orange dashed lines, TTX cryogels and areas targeted by blue dashed lines. (A') Schematic showing the placement of the cryogels (A) on a mouse brain tissue slice. (A'') The areas marked by the orange (control) and blue (TTX) boxes shown in (A) are shown for control and TTX applications prior to application and then 20 and 100 seconds after cryogel removal. (B) Repeat experiment as for (A) following washout of TTX. (C, D) Quantification of OGB fluorescence measured by integrated density as a ratio of the level of OGB fluorescence prior to application. This quantification was performed on mouse brain tissue slices that had one (C) or two (D) applications of cryogels. Statistical analysis: Error bars represent standard error (n = 4 (C), 3 (D)), two-way repeated-measures ANOVA, $F_{(1, 6)} = 9.467$, $p = 0.0218$, Treatment (Control vs TTX) (C), $F_{(1, 4)} = 28.91$, $p = 0.0058$, Treatment (Control vs TTX) (D). Scale bars 250 µm.